



Integrated Arctic Observation System

Research and Innovation Action under EC Horizon2020
Grant Agreement no. 727890

Project coordinator:
Nansen Environmental and Remote Sensing Center, Norway


Deliverable 3.6

First implementation and data: Greenland Data delivery and report on results of the observing systems in the coastal Greenland

Start date of project:	01 December 2016	Duration:	60 months
Due date of deliverable:	30 November 2019	Actual submission date:	28 November 2019
Lead beneficiary for preparing the deliverable:	GEUS		
Person-months used to produce deliverable:	23.53 PM		

Authors: Andreas P. Ahlstrøm, Robert S. Fausto, Michele Citterio, Jason E. Box, Masashi Niwano, Dirk van As, Mikael Sejr, Johnna Holding, Roberta Pirazzini, Teijo Arponen, Francisco Navarro, Javier Lapazaran, Laurent Chauvaud, Marcel Babin, Claudie Marec

Version	DATE	CHANGE RECORDS	LEAD AUTHOR
1.0	14.10.2019	Template	A. Beszczynska-Möller
1.1	27.11.2019	Final version	A.P. Ahlstrøm
1.2	28.11.2019	Revised and approved	P. Voss
1.3	28.11.2019	Technical review and submission	K. Lygre

Approval X	Date: 28 November 2019	Sign.  Coordinator
----------------------	---------------------------	--

USED PERSON-MONTHS FOR THIS DELIVERABLE					
No	Beneficiary	PM	No	Beneficiary	PM
1	NERSC		24	TDUE	
2	UiB		25	GINR	
3	IMR		26	UNEXE	
4	MISU		27	NIVA	
5	AWI		28	CNRS	X
6	IOPAN		29	U Helsinki	
7	DTU		30	GFZ	
8	AU	14	31	ARMINE	
9	GEUS	3.94	32	IGPAN	
10	FMI	4.09	33	U SLASKI	
11	UNIS		34	BSC	
12	NORDECO		35	DNV GL	
13	SMHI		36	RIHMI-WDC	
14	USFD		37	NIERSC	
15	NUIM		38	WHOI	
16	IFREMER		39	SIO	
17	MPG		40	UAF	
18	EUROGOOS		41	U Laval	
19	EUROCEAN		42	ONC	
20	UPM	1.5	43	NMEFC	
21	UB		44	RADI	
22	UHAM		45	KOPRI	
23	NORUT		46	NIPR	
			47	PRIC	

DISSEMINATION LEVEL		
PU	Public, fully open	X
CO	Confidential, restricted under conditions set out in Model Grant Agreement	
CI	Classified, information as referred to in Commission Decision 2001/844/EC	

EXECUTIVE SUMMARY

This document, ***Deliverable 3.6 - First implementation of the observing system: Data delivery and report on results of the observing systems for the Coastal Greenland***, describes the first implementation and results of use of INTAROS WP3 (Task 3.1) for the Coastal Greenland reference site, which is identified as a key location for freshwater output from the Greenland ice sheet to the ocean.

The activities reported here from Task 3.1 describe the first field deployments and results for both offshore, onshore and on-ice instrumentation to monitor identified environmental variables, including:

- *snow cover on sea ice* - for impact of freshening on the marine ecosystem
- *surface pCO₂ and ocean acidification* - for impact of freshening on CO₂-uptake of the ocean
- *snow-water equivalent on the ice sheet* - for reducing uncertainty in meltwater output to the ocean
- *precise positioning of ice sheet stations* - for calibration for satellite-derived ice velocity maps and numerical weather prediction
- *new radiometer tilt and azimuth instrument for improved radiation correction* – for improving radiometer data corrections
- *rain gauges on ice sheet stations* – for capturing the transition from snow to rain of the precipitation on the Greenland ice sheet
- *instrument characterization of in-situ ice sheet albedo measurements* – for better validation of satellite albedo products
- *Improvement of ice-penetrating radar system* - for generating ice thickness data over ice-sheet outlet glaciers
- *passive acoustics for characterization of both physical and biological parts of the marine ecosystem* – for studying the ice-driven dynamics of Arctic coastal ecosystems
- *improvement of under-ice monitoring* – for observations of spring bloom and bio-optical/-geochemical properties

Table of Contents

1. Introduction	6
2. First implementation and operational use of the observing system for the Coastal Greenland	7
2.1. GEUS	7
2.1.1.1. First results from adding automated measurements of snow water equivalent on the PROMICE weather station network	7
2.1.1.2. First results from high accuracy GNSS positioning	13
2.1.1.3. First results from the new radiometer tilt and azimuth instrument for improved radiation correction	18
2.1.1.4. First results from rain gauges on ice sheet AWS	20
2.1.2. Description of provided data	22
2.1.2.1. Data from automated measurements of snow water equivalent on the PROMICE weather station network	22
2.1.2.2. Data from high accuracy GNSS positioning	26
2.1.2.3. Data from the radiometer tilt and azimuth instrument for improved radiation correction	26
2.1.2.4. Data from rain gauges on ice sheet AWS	26
2.1.3. Plans for the final implementation	27
2.1.3.1. Plans for adding automated measurements of snow water equivalent on the PROMICE weather station network	27
2.1.3.2. Plans for high accuracy GNSS positioning	27
2.1.3.3. Plans for the radiometer tilt and azimuth instrument for improved radiation correction	27
2.1.3.4. Plans for rain gauges on ice sheet AWS	28
2.2. AU	28
2.2.1. Results of the first operational implementation	28
2.2.2. Description of provided data	31
2.2.3. Plans for the final implementation	32
2.3. FMI	32
2.3.1. Results of the first operational implementation	33
2.3.2. Description of provided data	34
2.3.3. Plans for the final implementation	34

2.4.	UPM	34
2.4.1.	Results of the first operational implementation	34
2.4.2.	Description of provided data	35
2.4.3.	Plans for the final implementation	37
2.5.	CNRS-IUEM	37
2.5.1.	Results of the first operational implementation	37
2.5.2.	Description of provided data	38
2.5.3.	Plans for the final implementation	38
2.6.	CNRS-Takuvik	38
2.6.1.	Results of the first operational implementation	38
2.6.2.	Description of provided data	39
2.6.3.	Plans for the final implementation	40
3.	Future plans for the final implementation of the observing system	42
4.	Summary	43
5.	Literature	46

1. Introduction

INTAROS aims to develop and implement innovative solutions and new technologies to fill selected gaps identified in the existing observing systems, as discussed in the WP2 gap assessment and prior efforts. The plan is to accomplish this aim by integration of novel instruments and sampling methods with mature components of existing observatories to increase temporal and geographic coverage of in situ observational data in the Arctic and include key parameters which are currently missing.

Three reference sites were selected within INTAROS as providing critical data to understand ongoing climate and environmental changes and their consequences for the Arctic. This report is focused on describing the technical development and system design phase in WP3 for one of these, namely Coastal Greenland, which is identified as a key location for freshwater output from the Greenland ice sheet to the ocean.

As the intention in WP3 is to optimize the fieldwork effort and maintain the integrity of new data, we will build on and effectively extend infrastructure already existing in selected reference sites and distributed observatories. Over the duration of the WP3 deployment phase, new sensors, integrated platforms and experimental setups will be implemented with the intention of sustained use in a future iAOS. Once in place, the new collected data will be pre-processed under WP3 to provide standardized data sets ready for integration in WP5, demonstration actions in WP6, and for the consultations with stakeholders in WP7.

The activities in the coastal region of Greenland covered in Task 3.1 on which this report is focused, includes a range of actions both offshore, onshore and on the Greenland ice sheet to monitor identified environmental variables. Specifically, these include

- A combination of ocean moorings with new solutions for the Northeast Greenland site to obtain coverage, duration, thickness and energy balance of snow cover on sea ice to increase knowledge of how freshening of the Arctic impacts the marine ecosystem.
- Establishment of an essential baseline dataset on surface pCO₂ and ocean acidification for the entire Greenland coastal zone, enabling future monitoring of the impact of freshening on CO₂ uptake of the ocean.
- Implementation of a novel ruggedized system adding to the existing on-ice PROMICE weather station network for measuring snow-water equivalent on the ice sheet margin, in order to capture meltwater retention mechanisms in the snow and firn on the ice; a main uncertainty in modelling of future ice sheet runoff and key to the meltwater output to the ocean from the Greenland ice sheet.

- Addition of precise positioning capability of the same on-ice sheet network will provide much needed calibration for satellite-derived ice velocity maps used to calculate the ice-dynamic mass loss to the ocean and monitor potential feedbacks between meltwater formation and ice dynamics.
- The addition of rain gauges to the in-situ PROMICE automatic weather stations on the Greenland ice sheet in order to capture the transition of a precipitation regime dominated by snow to one with frequent rain events.
- Improvement of the accuracy and spatial representativeness of the in-situ snow albedo observations (from PROMICE and GC-Net networks) over Greenland ice sheet through improved instrument characterization as well as a methodology for correction of in-situ ice sheet albedo measurements.
- Improvement of an innovative ice-penetrating radar system for generating ice thickness data over highly crevassed ice-sheet outlet glaciers.
- Implementation of a multi-disciplinary approach to study the ice-driven dynamics of the Arctic coastal ecosystems in the Young Sound (with similar system in Kongsfjorden under Task 3.3 for a comparison of two contrasted fjords), by merging physical oceanography and marine biology, and using the passive acoustics non-invasive technique to characterize both physical (dynamics of sea ice and icebergs, waves-ice interactions) and biological compartments (behavior of organisms at different trophic levels).
- Contribution to a suite of sensors for automated monitoring of the spring bloom processes and the bio-optical and biogeochemical properties under the ice pack of the coastal ocean at the Baffin Bay Observatory (in Qiqiktarjuak).

2. First implementation and operational use of the observing system for the Coastal Greenland

2.1. GEUS

Contributors: Robert S. Fausto, Michele Citterio, Andreas P. Ahlstrøm, Jason E. Box, Masashi Niwano, Dirk van As

2.1.1.1. First results from adding automated measurements of snow water equivalent on the PROMICE weather station network

SnowFox

The SnowFox measures snow water equivalent (SWE) through the attenuation of cosmic-ray neutrons. The sensor records neutron events over a regular interval. To derive SWE, the raw neutron counting rate of the sensor must be corrected for variations in barometric pressure and solar activity. The corrected neutron counting rate is then normalized to a no-snow reference counting rate. Any subsequent counting rate will decrease exponentially as a function of the amount of SWE overlying the detector.

Output files

Data files are stored on the removable SD card in ascii format. The compact binary files are used mostly for data telemetry and can otherwise be ignored. As a default for satellite transmissions, a new data file is created once every hour. This interval can be reset to a longer/shorter period, resulting in larger/smaller files.

The name of the file containing sensor data corresponds to the date and time it was created. The naming format is:

YYMMDDHHmm.EXT

where: YY = year, MM = month, DD = day, HH = hour, mm = minute, and EXT = the data logger extension number (as indicated in the QILogger.ini file). New files are automatically created at the start of each month, with filenames named again according to the YYMMDDHHmm.ext convention.

Converting counts to SWE

In general, the procedure is as follows.

(1) Correct the raw counting rate. Unwanted environmental effects are eliminated by applying a correction factor $F(t)$ to the raw counting rate, N_{raw} , such that the corrected counting rate is:

$$N = F(t) \cdot N_{raw}$$

The data logger only reports the raw counting rate, so the correction must be done by the user. The overall correction factor $F(t)$ can be decomposed into correction factors for the individual processes. Currently the main correction factors account for barometric pressure (f_{bar}) and solar activity (f_{sol}). The total correction factor is thus:

$$F(t) = f_{bar} \cdot f_{sol}$$

The first of these is the barometric pressure correction factor, calculated as

$$f_{bar} = \exp[\beta \cdot (P(t) - P_0)]$$

where $P(t)$ is the barometric pressure recorded at the site in hPa, P_0 is a fixed reference pressure in hPa, usually taken to be an approximate long term average for the site, or calculated from the elevation and a model representation of the atmosphere. The choice of P_0 is somewhat arbitrary, but must be consistent while processing the time series. β is the pressure coefficient, which at high to mid latitude can be assumed to be 0.0077 hPa^{-1} .

The second factor corrects for variations in solar activity, and is calculated as

$$f_{sol} = \frac{M_0}{M(t)},$$

where $M(t)$ is the counting rate of a neutron monitor at time t , and M_0 is the counting rate at an arbitrarily chosen reference time. (The idea is to normalize all counting rates to a single reference solar activity level; the exact reference level chosen is not important as long as the user is consistent). The factor f_{sol} is calculated on an hourly basis and reported on a Hydroinnova maintained web portal, <http://nearfld.com/reguser/solar/>. This correction factor is most accurate for high altitude sites in Europe.

Calculate the effective attenuation length, L , in water. We use the formula:

$$\frac{1}{L} = \frac{1}{L_{max}} + \left(\frac{1}{L_{min}} - \frac{1}{L_{max}} \right) \cdot \left(1 + \exp \left[-\frac{\frac{N}{N_0} - a_1}{a_2} \right] \right)^{-a_3}$$

For a SnowFox installed on the ice sheet, the recommended parameters are shown in Table 2.1.1.

Table 2.1.1. Recommended snowfox parameters for correcting raw neutron count on ice from the manufacturer.

L_{max}	1.354×10^2 [cm]
L_{min}	1.701×10^1 [cm]
a_1	3.071×10^{-1}
a_2	6.330×10^{-2}
a_3	0.6029

We then calculate SWE from the exponential attenuation relationship:

$$SWE = -L \cdot \ln \left(\frac{N}{N_0} \right)$$

Here N_0 is the initial “snow free” counting rate. If L is in centimeters then the resulting SWE will also be in centimeters.

Since PROMICE AWSs primarily set out to monitor melt and its atmospheric forcings, the stations are commonly located in high-melt regions where equipment melts out and the uneven terrain affects station stability. The ongoing cycles of freezing and thawing, and the powerful katabatic winds and winter storms are harmful to instruments. We therefore visit all stations every one to four years, balancing cost, necessity and opportunity.

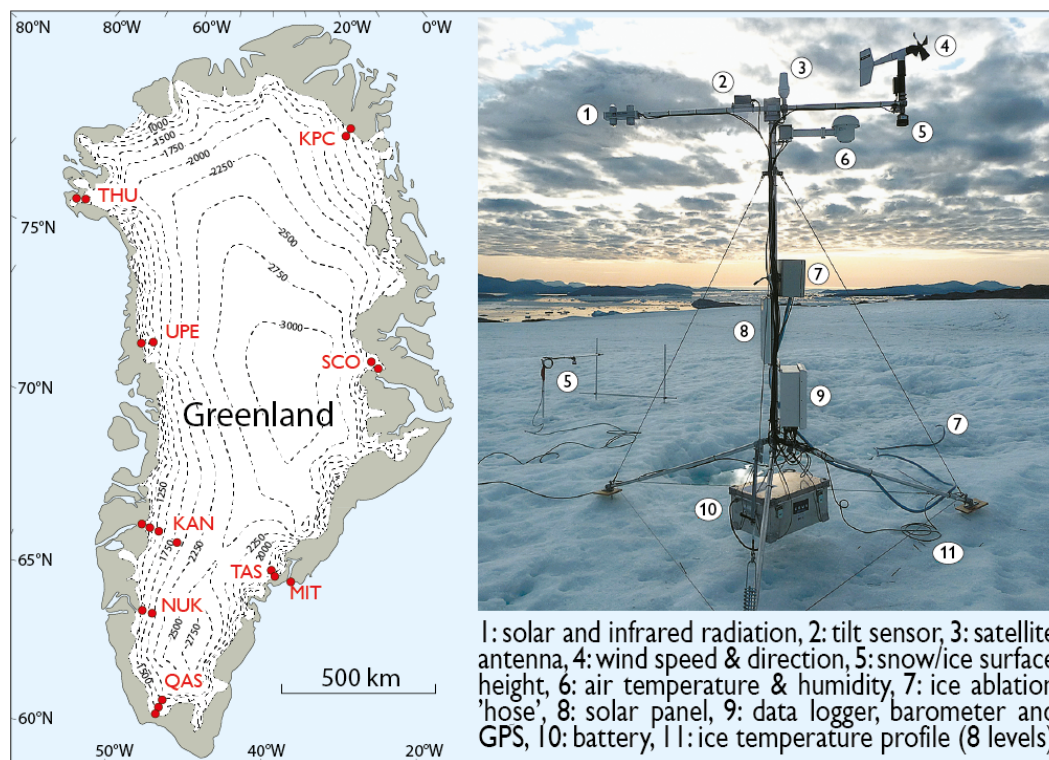


Figure 2.1.1. PROMICE locations with AWSs at different elevations (left). PROMICE AWS UPE_L photographed on 17 August 2009.

Snowfox status 2019

In 2018, we installed five snowfoxes at four PROMICE locations, namely Tasiilaq (TAS), Qassimiut (QAS), Kangerlussuaq (KAN), and Thule (THU) (Figure 2.1.1). Two sensors were deployed at the QAS transect at different elevation to measure the altitudinal gradient in SWE. Initial testing of the system and sensor found an optimal configuration for deployment onto the ice sheet. The optimal configuration was a 4-hour counting period every other day to conserve power. We mounted the SnowFox loggerbox on a “stand alone” PROMICE tripod together with a solar panel and a battery box with six Panasonic (28 Ah, in total 156 Ah) batteries inside (Figure 2.1.2). The SWE sensor (SnowFox) was placed next to the tripod on ice so that it could be buried by snow during the accumulations season. During the 2019 field season, we retrieved the data from all deployed SnowFoxes, but we had some problems with power in four places because of either too much snow that buried our solar panel or too little sunlight in the winter months to recharge the batteries (Figure 2.1.3).

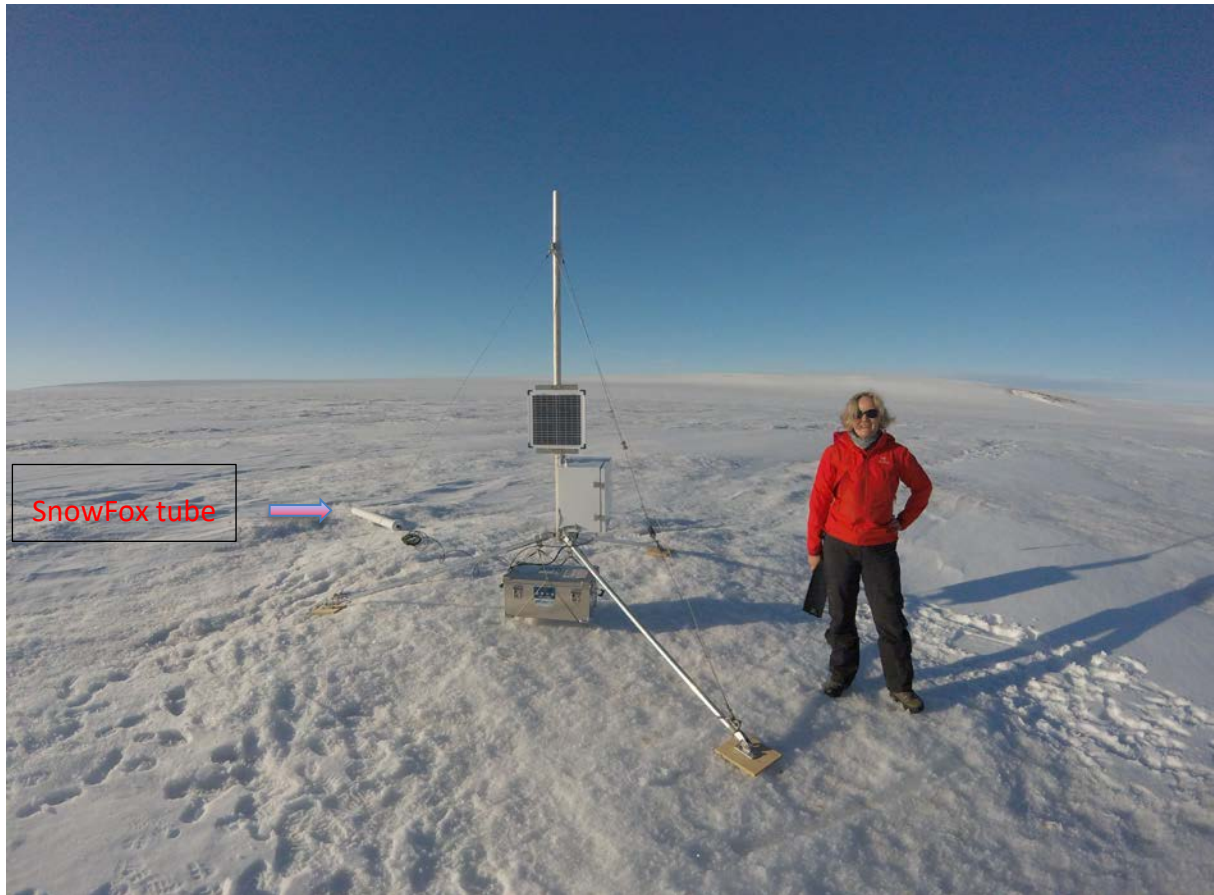


Figure 2.1.2. SnowFox at the TAS_A site end of summer 2018.



Figure 2.1.3: SnowFox at the TAS_A site spring 2019.

2.1.1.2. First results from high accuracy GNSS positioning

The instrument provides L1/L2 dual frequency code and carrier phase logging (GPS and GLONASS) as well as standalone positioning, based on the AsteRx-m receivers by Septentrio (Leuven, Belgium) and also supports the newer AsteRx-m2 modules which add reception of the L5 frequency and Galileo signals. The instrument designed for INTAROS includes a control board managing power supply, data logging on a removable micro-SD flashcard formatted with a FAT32 filesystem, serial communication for interfacing with a Campbell CR1000 datalogger as used on the PROMICE automatic weather stations (AWS), as well as a realtime clock to also allow autonomous operation independent from an AWS. The receiver module is controlled through and plugs onto the control board using multi-pins connectors carrying power and the digital signals. The coaxial cable carrying the radio signal from the antenna is instead connected directly to the receiver module in order to reduce signal losses. The antenna is a Pinwheel type by Novatel (Canada) connected through a short coaxial cable terminated with a TNC connector on the antenna side and an N connector on the instrument side. When connected to an AWS, Iridium satellite data transmission is available through the station. When operating independently, data transmission is provided by a separate module which is currently under development. Power constraints and expensive satellite airtime fees make transmitting the raw code and phase logs impractical, therefore transmission is limited to time, latitude, longitude, elevation and optionally a set of diagnostic parameters. The close distance between the Iridium and GNSS antennas and on the instruments boom opens the possibility of interference on the L1 band, especially for GLONASS (1593-1610 MHz, right-hand polarized) from the adjacent Iridium up/downlink frequency allocation (1621.35-1626.5 MHz, right-hand polarized) when the transmitter is active. The passive GNSS antenna we use has a -3 dB passband of 1.15-1.65 GHz and doesn't provide significant attenuation of the interfering signal except for the gain roll-off near the horizon, but the lack of amplification also reduces the risk of overload damage to the receiver. Limited testing was done prior to the 2019 field deployment by operating an Iridium 9602 SBD transceiver feeding an SAF5350-A antenna located at the same height and the side of the GNSS antenna, with a clearance of 20 cm between them. No loss of tracking was observed on the receiver, but closer inspection of the logged code and phase data are needed to confirm interference is negligible. Because SBD transmissions only transmit for very brief time, another test was done with a commercial Iridium handset by making a 1 minute voice call, again with 20 cm air gap between the handset antenna and the GNSS antenna. In this case, loss of tracking was observed for some satellites, but no evidence of overload damage. Similar interference problems have been previously reported (<https://connect.unavco.org/display/pub678802>).

The specifications of the INTAROS instrument match or exceed the stated design goals from the 2018 INTAROS D3.1 report:

- data rate: record for 2 hours and deliver at least one accurate position per day in winter, record 24/7 and deliver up to one accurate position per hour in summer.
- accuracy: 0.5 m 1σ (within 24 hours from observation), cm-scale (postprocessed)

- data storage: 2 years of data
- power: run on less than 500 Wh of battery power through the polar night, on solar power during summer
- communication: serial communication to GEUS AWS and Iridium SBD satellite service
- system configuration: standalone or connected to a PROMICE AWS



Figure 2.1.4. The INTAROS high accuracy GNSS instrument and power supply are contained in the black anodized aluminum enclosure mounted on the instrument boom of the NUK-K PROMICE AWS. The Novatel Pinwheel antenna and the 2 W solar panel are also visible.

The field implementation started in summer 2019, Fig. 2.1.4 shows a unit installed on the NUK-K station (N 64.1°, W 51.3°). While the deployment is on the instruments boom of a standard PROMICE AWS, the INTAROS unit is configured to operate completely independently from the AWS in order to avoid for this initial field deployment any risk of malfunctions disturbing the normal operation of the AWS. This is made easy by the very low power consumption of the INTAROS instrument which allows fitting the receiver, control board, and battery power supply within a small IP-67 rated metal enclosure.

The measured power consumption of the complete instrument is given in Table 2.1.2 for both the dual frequency and triple frequency receiver modules AsteRx-m and -m2. The triple frequency has significantly higher power consumption, but the dual frequency variant has been discontinued by the manufacturer. Recording the third frequency and the Galileo signals is beneficial during postprocessing resulting in similar positioning accuracy with a shorter recording time compared to the discontinued dual frequency GPS+GLONASS only receiver, so that the overall system power requirements as configured for wintertime operational use is similar irrespective of the module used. Power consumption measured under different operational states is listed in Table 2.1.2.

Table 2.1.2, power consumption (2.5 V < supply voltage < 18 V unless otherwise stated)		
INTAROS GNSS receiver, dual frequency	Measurement condition	Average power consumption
L1, L2 logging (GPS, GLONASS)	5 sec., see Table 2.1.3 for details	0.7 W
standby		2 mW
time-keeping only	no supply voltage (needs backup battery)	0.1 mW
INTAROS GNSS receiver, triple frequency		average power consumption
L1, L2, L5 logging (GPS, GLONASS, Galileo)	5 sec., see Table 2.1.3 for details	1.1 W
L1, L2 logging (GPS, GLONASS)	5 sec., L5 and Galileo disabled	0.9 W
standby		2 mW
time-keeping only	no supply voltage (needs backup battery)	0.1 mW

In the configuration shown in Fig. 2.1.4 a 6V, 2W solar panel is mounted directly on the enclosure and is dimensioned to work through the polar night at the latitude of Nuuk, Greenland (64.15N) with a small 6V, 70 Wh lead-acid battery. A larger solar panel will be needed for 24/7 summertime operation and a larger battery for wintertime operation at higher latitudes. The detailed configuration of the receiver is listed in Tab. 2.1.3 where all non-default settings are shown for the AsteRx-m2 variant, the Galileo and L5 settings not being supported by the AsteRx-m variant.

Table 2.1.3, receiver configuration	
Septentrio AsteRx module setting	comment
setSBFOutput, Stream1, DSK1	enable logging of SBF-formatted data to flashcard

setSBFOutput, Stream1, , MeasEpoch+GPSNav+GPSIon+GPSUtc+GLONav+GALNav+GALUtc+GALGstGps+GEONav+PVTGeodetic+ReceiverSetup+Comment+BDSNav+QZSNav	select the measurements to be logged in the SBF-formatted file on the flashcard
setSBFOutput, Stream1, , , sec5	set the SBF-formatted data rate to 5 s
setNMEAOutput, Stream1, DSK1	enable logging of NMEA-formatted data to flashcard
setNMEAOutput, Stream1, , GGA	select NMEA GPGGA data format
setNMEAOutput, Stream1, , , sec5	set the NMEA GPGGA-formatted data rate to 5 s
setSmoothingInterval, GPSL1CA, 1000	set carrier smoothing interval of GPSL1CA code to 1000 s
setSmoothingInterval, GPSL2PY, 1000	set carrier smoothing interval of GPSL2PY code to 1000 s
setSmoothingInterval, GPSL2C, 1000	set carrier smoothing interval of GPSL2C code to 1000 s
setSmoothingInterval, GPSL5, 1000	set carrier smoothing interval of GPSL5 code to 1000 s
setSmoothingInterval, GLOL1CA, 1000	set carrier smoothing interval of GLOL1CA code to 1000 s
setSmoothingInterval, GLOL2P, 1000	set carrier smoothing interval of GLOL2P code to 1000 s
setSmoothingInterval, GLOL2CA, 1000	set carrier smoothing interval of GLOL2CA code to 1000 s
setSmoothingInterval, GLOL3, 1000	set carrier smoothing interval of GLOL3 code to 1000 s
setSmoothingInterval, GALL1BC, 1000	set carrier smoothing interval of GALL1BC code to 1000 s
setSmoothingInterval, GALE5a, 1000	set carrier smoothing interval of GALE5a code to 1000 s
setSmoothingInterval, GALE5b, 1000	set carrier smoothing interval of GALE5b code to 1000 s
setSmoothingInterval, GALE5, 1000	set carrier smoothing interval of GALE5 code to 1000 s
setSmoothingInterval, GEOL1, 1000	set carrier smoothing interval of GEOL1 code to 1000 s
setSmoothingInterval, GEOL5, 1000	set carrier smoothing interval of GEOL5 code to 1000 s
setElevationMask, PVT, 5	set the satellite elevation mask to 5 degrees
setReceiverDynamics, Low	set the receiver dynamic model to Static Low
setReceiverDynamics, , Static	set the receiver dynamic model to Static Low
setObserverParameters, "micit@geus.dk"	set user metadata
setObserverParameters, , "GEUS"	set user metadata
setFileNaming, DSK1, IGS1H	set filename convention to IGS/RINEX hourly files
setWakeUpInterval, "2019-01-01 11:55:00"	set the starting point for optional self-timed operation
setWakeUpInterval, , 11100	set the duration of optional self-timed operation to 3 hours
setWakeUpInterval, , , 86400	set the repetition of optional self-timed operation to 1 day
setLBandSelectMode, off	Turn off demodulation of L band augmentation signals

To assess the feasibility of using a passive antenna instead of a more conventional active one, the performance of the receiver connected through a 40 cm low loss coaxial cable to a Novatel GPS-704-X passive antenna has been compared with a similarly connected Novatel GPS-703-GGG. Both antennas were connected to their respective input connectors on the receiver during the entire duration of the test, and the receiver was switched from using one or the other through software configuration.

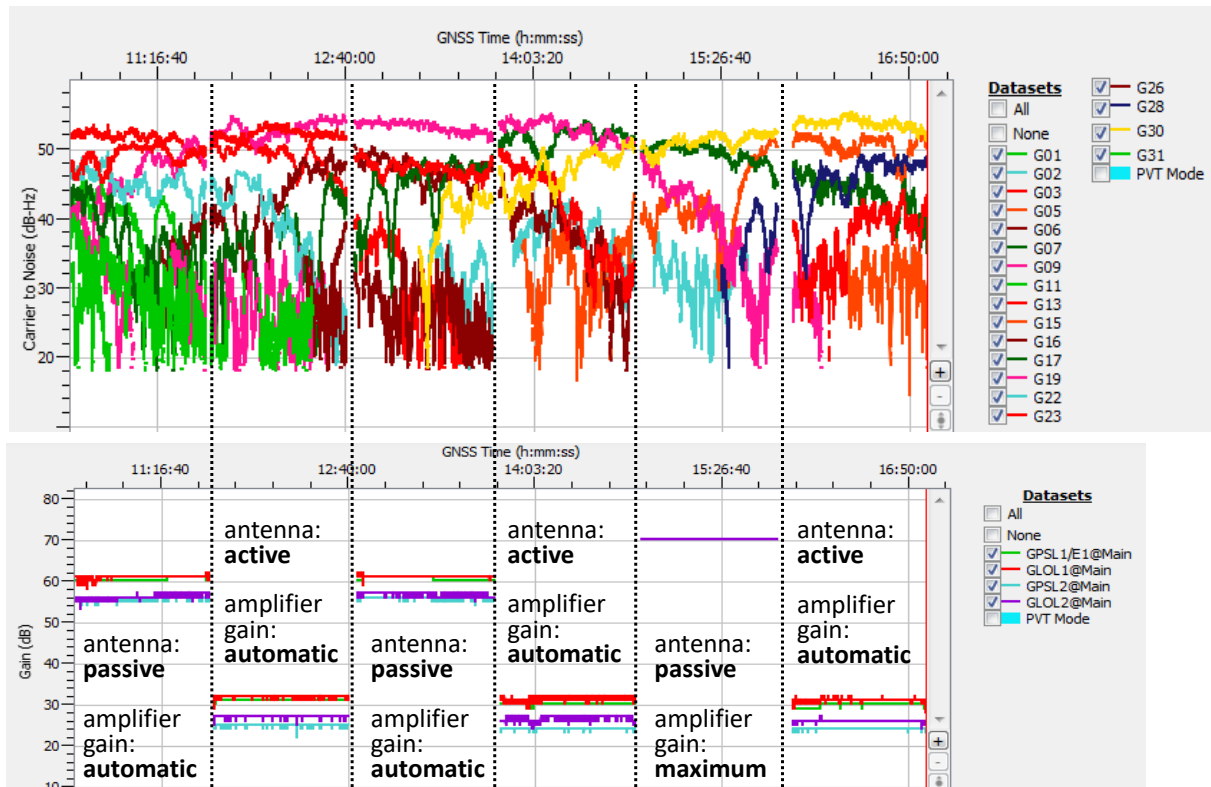


Figure 2.1.5. Test of receiver performance using an active vs. passive antenna and different settings of the frontend LNA amplifier, showing the carrier ratio with the passive antenna to be adequate.

The results of one such tests spanning several hours and different settings of the low noise amplifier (LNA) in the receiver frontend show that the reduction in carrier to noise ratio is minor (Fig. 2.1.5) and that the receiver still tracks all signals irrespective of the antenna type (Fig. 2.1.6). These tests were done early when only the Septentrio AsteRx-m version was available, but they also apply to the -m2 version which according to the manufacturer specifications is more sensitive (tracking threshold 20 dB-Hz vs. 26 dB-Hz, acquisition is specified as 33 dB-Hz for both versions).

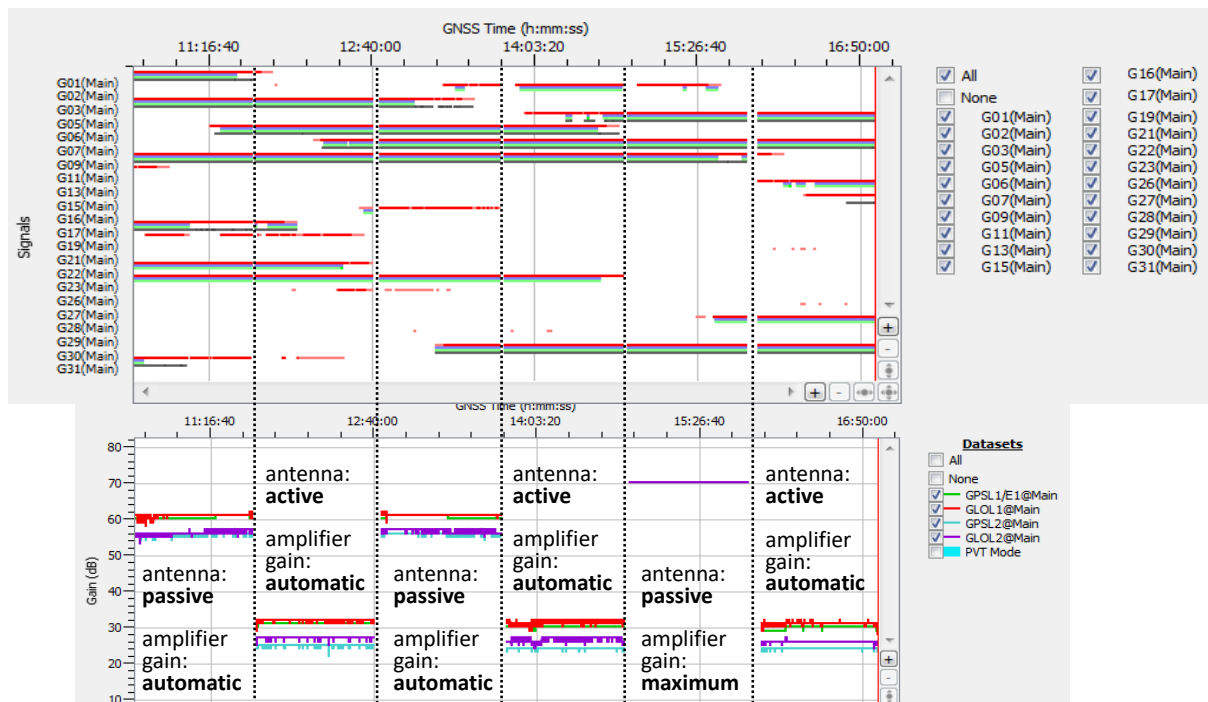


Figure 2.1.6. Test of receiver performance using an active vs. passive antenna and different settings of the frontend LNA amplifier, showing the ability of the receiver to track all GPS and GLONASS signals both with the passive and the active antenna.

2.1.1.3. First results from the new radiometer tilt and azimuth instrument for improved radiation correction

The instrument measures the tilt and azimuth of the Kipp & Zonen CNR-1 and CNR-4 radiometers carried by the PROMICE AWS. This is needed to correct the radiation measurements because AWS operating on ice cannot provide a stable level orientation of the radiometers. The INTAROS instrument is composed of a control board carrying a precision 2-axes accelerometer and tilt meter type ADIS16209 by Analog Devices (USA) and a solid state electronic compass type HMC6343 by Honeywell (USA). The HMC3443 is also capable of measuring tilt, however not at the sub-degree accuracy required by our application. The tilt information from the HMC6343 is therefore only used internally as a confidence check for the ADIS16209 measurements and as a fallback in case the ADIS16209 fails.

The specifications of the instrument match or exceed the stated design goals from the 2018 INTAROS D3.1 report:

- data rate: measure 2-axes tilt and magnetic azimuth every 10 minutes both in winter and summer.
- accuracy: 0.3 degrees pitch and roll, 3 degrees magnetic heading
- data storage: none (relies on attached GEUS AWS as used by PROMICE)
- power: consume less than 100 mW when powered on
- communication: serial communication to the GEUS AWS

- system configuration: mechanically mounted on the radiometer body and electrically connected to a GEUS AWS

The development of this sensor was delayed in the first half of 2019 due to problems with powering and interfacing to the ADIS16209 resulting in occasional lock-ups during testing, as well as difficulties implementing the planned serial communication using the SDI-12 protocol. To sidestep the difficulties with implementing the SDI-12 protocol and to speed up the adoption of the new INTAROS instrument at as many GEUS AWS as possible, an analog output interface has been added that mimics the output signals of the 2-axes tilt meter currently in use. Between 25 degrees from the horizon on each axis, the analog output is proportional to the tilt and ranges between -2.5 and +2.5 V with a linear coefficient of $10^\circ/\text{V}$. This matches the full range covered by the previous sensor used on the GEUS AWS, and without requiring the linearization correction needed by the older sensor.

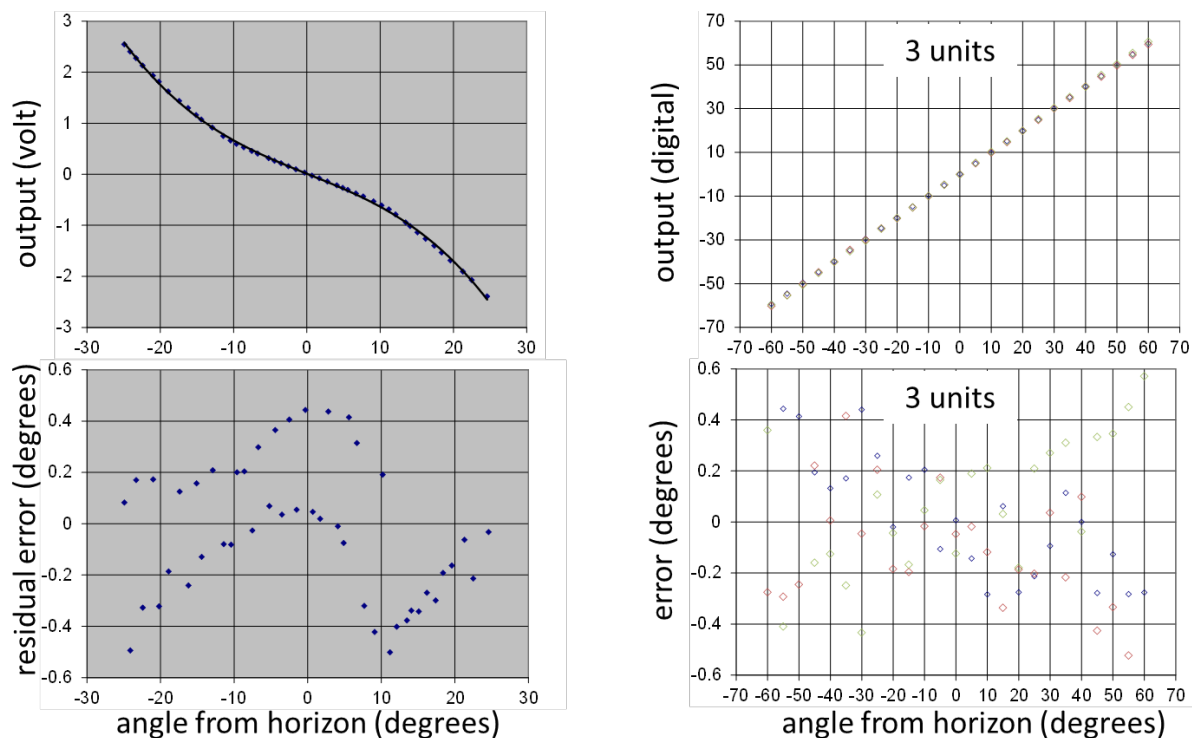


Figure 2.1.7. Comparison of tilt and tilt error measured with the current sensor used on the GEUS AWS (left) and the new INTAROS sensor (right).

The INTAROS instrument can measure all the way to +/- 90 degrees and even though the quality of the radiation correction at steep angles is poor, high inclination is important diagnostic information for the planning of the field maintenance visits. For this reason the INTAROS device also outputs angles between 25 and 90 degrees with no loss of resolution through the serial interface and with a linear coefficient of 30°/V on the analog interface. A performance comparison in the lab between 3 different INTAROS prototype units and the tilt sensor currently used on the GEUS AWS is shown in Fig. 2.1.7, where the residual error of the old sensor is plotted after correction for the non-linear response while the INTAROS instrument does not require such correction. The INTAROS hardware supports an improved correction for non-zero offset at level angle and for measurement of drift due to temperature fluctuations, but these have not yet been implemented in the firmware. The power consumption is indicated in Table 2.1.4.

Table 2.1.4, power consumption (5.3 V < supply voltage < 30 V unless otherwise stated)		
INTAROS tilt and azimuth	Measurement condition	Average power consumption
actively measuring, all outputs active	first 5 sec. from power-up, 0 output current	40 mA
measurement paused, all outputs active	0 output current	5 mA

The field implementation started in summer 2019 without the final mechanical housing of the sensor being ready and therefore it was included in the same aluminium enclosure also containing the INTAROS high accuracy GNSS receiver, which also includes power supply and a data logging (Fig. 2.1.4). While this setup is different from the final mechanical assembly intended to be accurately aligned with the body of the radiometer, it allows testing under field conditions and keeps the new instrument separate from the operational AWS so that any malfunction will not affect it.

2.1.1.4. First results from rain gauges on ice sheet AWS

While rainfall onto Greenland ice sheet has been measured in very few cases (e.g. Box et al. 2012; Niwano et al. 2015), it likely has strong impacts on surface melt processes. For example, rain transfers heat to snow and ice, possibly bringing earlier melt onset. Rain on snow causes snow grain growth with consequence of increased sunlight absorption; thus an amplifying feedback for melting.

Liquid precipitation data were obtained from six PROMICE locations (Fig. 2.1.8) using HOBO RG3-M rain gauges (<https://www.onsetcomp.com/products/data-loggers/rg3-m>) mounted on the PROMICE AWS mast 25 cm below the level of wind speed measurements (Fig. 2.1.8).

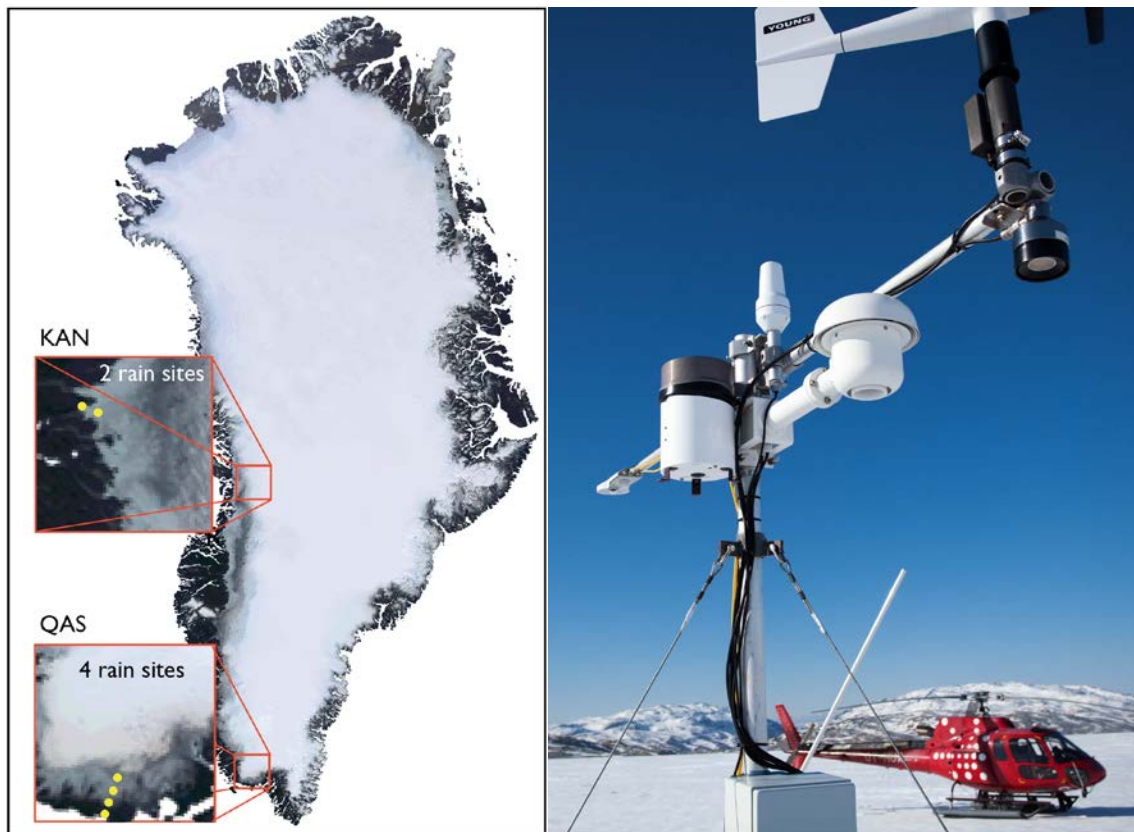


Figure 2.1.8. location map (left), Greenland ice sheet rain gauge locations and (right) example illustration of rain gauge placement near the top of the PROMICE AWS mast.

Some data issues remain:

- The deployed gauges, when buried or after heavy snowfall, will present a “rain” measurement that includes some effect of delayed snow melt. This “snow effect” may be ruled out in our case by attention to coincident temperature records and other information such as surface height records.
- There is a substantial undercatch expected from the distortion of the wind field around the rain gauge and the measurement platform. We thus apply a correction scheme designed to compensate from imperfect catch efficiency, based mainly on wind speed data from the weather station.

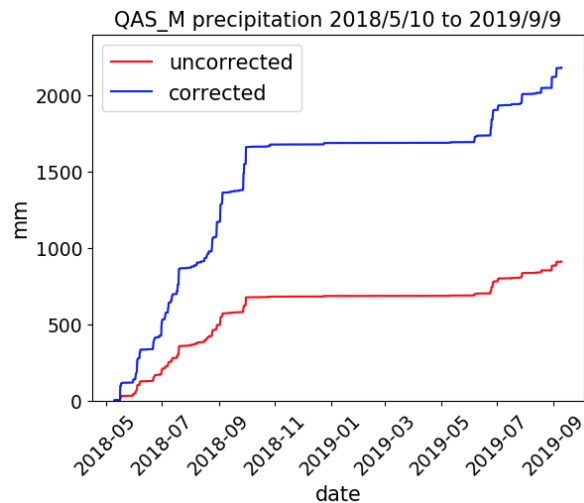


Figure 2.1.9. An example of uncorrected and corrected rain gauge data from the QAS-M location in ablation zone of the southernmost part of the Greenland ice sheet.

2.1.2. Description of provided data

2.1.2.1. Data from automated measurements of snow water equivalent on the PROMICE weather station network

The SnowFox records neutron events over a regular interval, usually one-six hours. In order to derive SWE, we first correct the raw neutron counting rate for variations in barometric pressure and solar activity, then normalize this corrected rate to a no-snow reference counting rate. The counting rate decreases as a function of the amount of SWE overlying the detector. As an example, we highlight the KAN_M site for the description of the SWE data. Following the above conversion procedure, we managed to convert raw counts (N1Cts) to SWE (Figure 4). Figure 4 illustrates the results: the top panel shows the raw and corrected counts, which is used to calculate SWE based on above conversion procedure second panel. The correction substantially smooths the variability of the measured count rate. The two bottom panels show measured snow surface height from the PROMICE AWS (we have two SR50A on our AWS setup), which are used together with the SnowFox SWE measurement to calculate the bulk snow density:

$$\rho_{snow_bulk} = \frac{SWE \cdot \rho_{water}}{H_{AWS}}$$

Starting from $N_0=8500$ the sensor was lying on the bare ice surface. Since the first snowfall event in mid September 2018 the count rate dropped to around 4000 by the end 2018, where it stayed relatively constant. Figure 2.1.10 shows that with an increasing amount of snowcover through the winter season follows the evolution of the SWE measurement when the SnowFox tube is fully covered in snow. However, calculating the bulk snow density for periods where the SnowFox tube is not fully covered in snow (SWE below 10 cm W eq.) results in much variability, which may not necessarily reflect the real changes in the snow density. Further, the snow height measurements from the PROMICE stations are recorded more than 10 meters away and may not be fully representative of the snow height over the SWE sensor during the whole winter season. The SWE changes in snow accumulation and snow melt at PROMICE sites completes the daily-weekly surface mass balance estimates for the whole year. Further, Figure 2.1.11 illustrates the problems with power in at QAS_U because of too much snow that buried our solar panel could not recharge the batteries (2019-01-06 was last measurement before burial). When the snow melted away the solar panel could recharge the batteries again and the SWE measurements started again (2019-06-16 was the first measurement after snow free solar panel). This indicates at the QAS_U site that most of the melt from the surface in the unmeasured period refroze close to its origin because the calculated density were almost 20 % higher when comparing density at the dates 2019-01-06 and 2019-06-16, respectively. The three other sites (QAS_M, TAS_A, THU_U2) also show promising result similar to those presented in Figures 2.1.10 and 2.1.11.

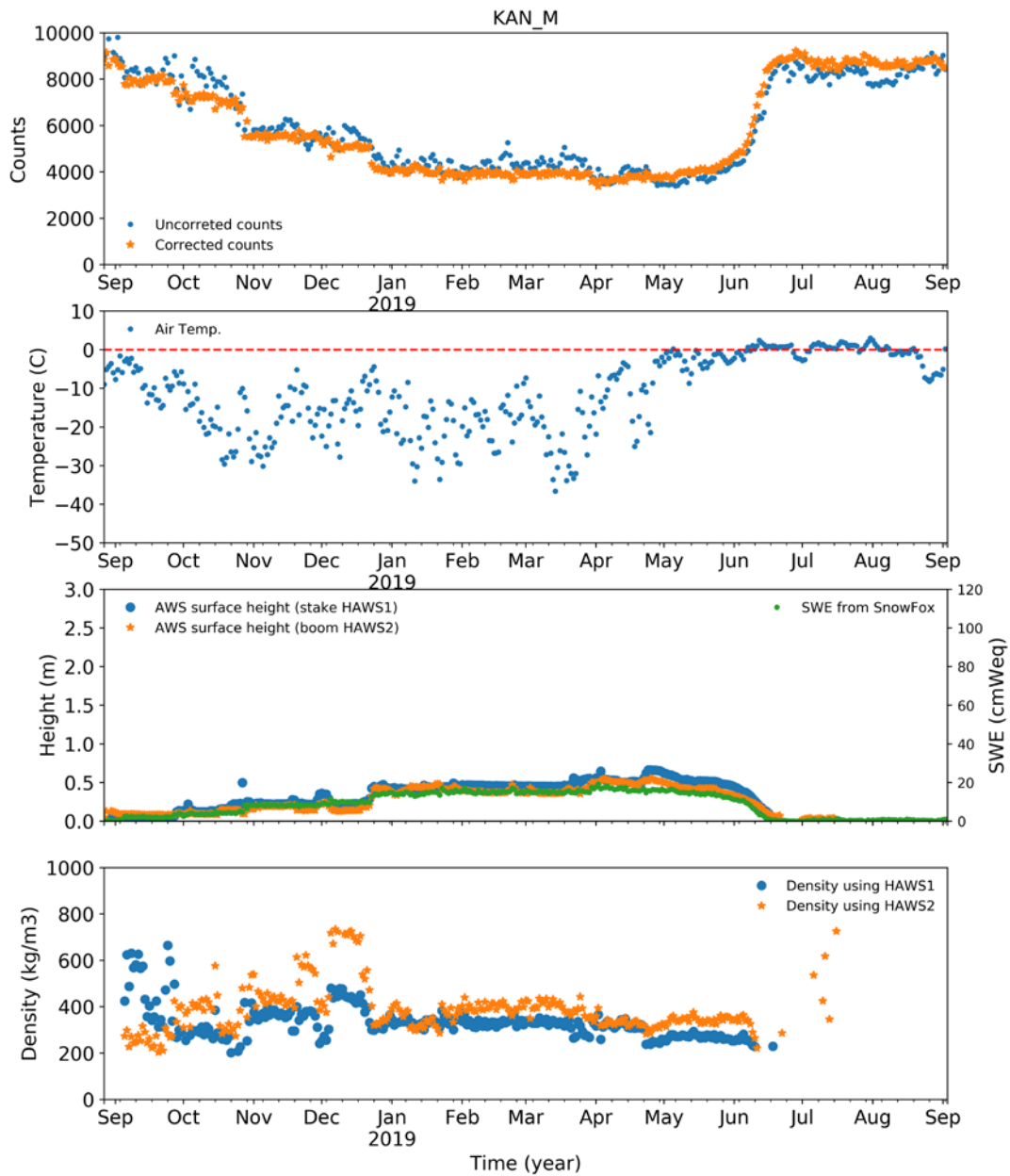


Figure 2.1.10. KAN_M site: Top panel shows the raw and corrected counts from the SWE sensor. Second panel shows observed air temperature. Third panel shows the two snow height measurements from the nearby PROMICE AWS and the calculated SWE. Fourth panel shows the calculated bulk snow density using SWE and snow height measurements.

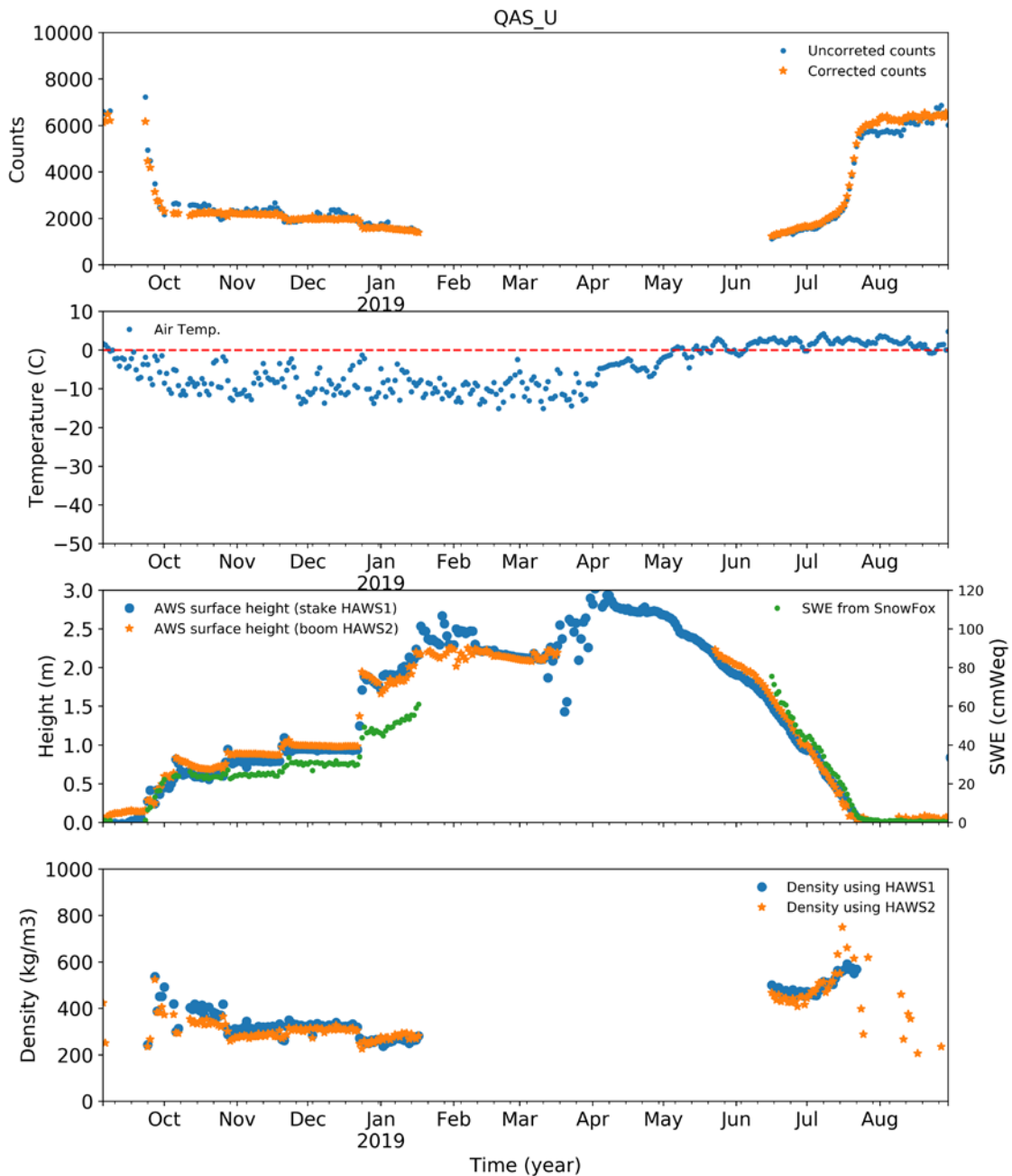


Figure 2.1.11. QAS_U site: Top panel shows the raw and corrected counts from the SWE sensor. Second panel shows observed air temperature. Third panel shows the two snow height measurements from the nearby PROMICE AWS and the calculated SWE. Fourth panel shows the calculated bulk snow density using SWE and snow height measurements.

As soon as the processed data has been properly quality controlled and validated, we will distribute the data on the PROMICE data portal.

2.1.2.2. Data from high accuracy GNSS positioning

Two different types of data are produced by the INTAROS high accuracy GNSS positioning instrument: standalone positions available directly from the instrument in the field, and raw code and carrier phase observables meant for postprocessing of positions with cm-scale accuracy. The standalone positions are output in the standard NMEA GPGGA format, which has been supported by the PROMICE AWS since 2008 for use with the previous single frequency GPS receivers. The raw code and carrier phase observables are logged on the flashcard using the Septentrio SBF format. This is a proprietary but fully documented format which is very compact to store on the instrument flashcard. An option is available to save in the standard RINEX v2.1 format which however uses several times more memory for the same information. Irrespective of the SBF or RINEX data format being logged, each recorded data file is named following the IGS/RINEX convention with the filename automatically changing every hour. After retrieving the logged data from the field the SBF-formatted files can be converted to standard IGS/RINEX either version 2.10 or 2.11 or 3.03 using the 'SBF Converter' utility available at <http://www.septentrio.com> for free download. The resulting files are compatible with postprocessing software (at GEUS we have a license for the Novatel Grafnet/Grafnav software and we also use the open source RTKLib).

The raw and processed data will be stored in the PROMICE database at GEUS and disseminated through the promice.dk website.

2.1.2.3. Data from the radiometer tilt and azimuth instrument for improved radiation correction

The INTAROS instrument outputs 2-axes tilt from horizontal and azimuth from the magnetic north pole as analog voltages as well as digital values in decimal degrees with a resolution of 0.1 degree. The tilt angles are used for correcting radiation measurements following the same well-established procedure as currently used by PROMICE with the lower accuracy measurements from the existing sensor. The availability of azimuth measurements will finally allow correcting for the unknown rotation that we have observed to occur at several AWS during the melt season. The INTAROS instruments internally runs a number of self-checks to verify the sensors are producing reasonable measurements and the error codes can be read through the SDI-12 interface and should be used for quality control.

The raw and processed data will be stored in the PROMICE database at GEUS and disseminated through the <http://promice.dk> website.

2.1.2.4. Data from rain gauges on ice sheet AWS

The data from the rain gauges are provided as five column comma-separated ASCII text (i.e., .csv files):

- a. Date, e.g. 2016-08-11 19:58:11
- b. Celsius air temperature, e.g. 3.72

- c. meters per second wind speed, e.g. 3.35
- d. mm water equivalent un-corrected precipitation, e.g. 0.2
- e. mm water equivalent corrected precipitation, e.g. 0.3

The rain gauge data are not presently transmitted as they are at the experimental state.

The amount of data so far analysed comprises 23494 precipitation “events”, equivalent each with a 0.2 mm increment.

The necessary corrections to precipitation gauge catch efficiency are after Goodison et al (1998) will be presented in Box et al (in preparation).

2.1.3. Plans for the final implementation

2.1.3.1. Plans for adding automated measurements of snow water equivalent on the PROMICE weather station network

We plan to adjust the system so that it measures for a longer period of time before sensor and datalogger goes into powersave mode. The SnowFox snow water equivalent (SWE) measurements will still be kept as separate systems along side the PROMICE station in order not to jeopardize the core station operation. Eventually, the SnowFox will be integrated in the standard station setup and established at all the stations where these parameters are relevant.

2.1.3.2. Plans for high accuracy GNSS positioning

The remaining of the units needed for the final implementation will be built and tested before the 2020 field season. The currently missing functionality in the firmware of the INTAROS high accuracy GNSS positioning will be implemented before deployment. These are primarily the software support of the SDI-12 serial protocol to enable communication with the Campbell datalogger in the AWS.

We plan to install more INTAROS high-accuracy GNSS units at the PROMICE and GlacioBasis AWS we will visit during the 2020 field season. The operational data processing will then start once the logged data are downloaded.

2.1.3.3. Plans for the radiometer tilt and azimuth instrument for improved radiation correction

The remaining of the units needed for the final implementation will be built and tested before the 2020 field season. The currently missing functionality in the firmware of the INTAROS tilt and azimuth will be implemented before deployment. These are primarily the software support of the SDI-12 serial protocol to enable communication with the Campbell data logger in the AWS. The mechanical assembly and weatherproof enclosure of the INTAROS tilt and azimuth device will also need to be finalized before the 2020 field season.

We plan to install more INTAROS tilt and azimuth instrument units at all the PROMICE and GlacioBasis AWS we will visit during the 2020 field season. The operational data processing will start without delay because the measurements will be transmitted via Iridium satellite link together as part of the operational near-real-time telemetry.

2.1.3.4. Plans for rain gauges on ice sheet AWS

The operation of rain gauges is to be continued through implementation of gauges on all (currently 22) PROMICE automatic weather stations (AWS). The measurements described here are pre-operational, i.e., test phase. That testing should produce standard version of PROMICE AWS to be phased-in starting in 2021. Once on PROMICE AWS, the values will be transmitted near-real-time by satellite data telemetry.

2.2. AU

Contributors: Mikael Sejr, Johnna Holding

2.2.1. Results of the first operational implementation

Seasonal data from Young Sound. The seasonal coverage of sea ice combined with turbidity associated with glacial runoff in summer are two essential parameters determining the amount of solar energy available for marine primary producers in Greenland fjords (Holding et al. 2019). As a consequence, spatial and interannual differences in sea ice cover and thus light availability have direct effects on the production of key species (Krause-Jensen et al. 2012). To improve the existing monitoring program in Young Sound, and our understanding of how meltwater input from the Greenland Ice Sheet determine marine light climate, INTAROS funded two new instruments to quantify the seasonal variation in turbidity and underwater light in the fjord. Since sea ice coverage and turbidity varies locally, the goal was to determine conditions at two sites; inner fjord, where sea ice appears to have lower snow cover, breaks up early July and where turbidity is high in summer due to runoff from several glaciers. Outer fjord, where sea ice breaks up in mid-July and where turbidity is relatively low (Fig. 2.2.1). Both instruments were deployed on August 13, 2018 and retrieved on August 3, 2019. Two types of instruments were purchased: for the outer fjord site a CTD (RBR Maestro) measuring temperature, salinity, depth, PAR (Photosynthetically Active Radiation), fluorescence (proxy for chlorophyll a biomass), dissolved oxygen and turbidity. For the inner fjord a CTD (RBR Concerto) measuring temperature, salinity, depth, PAR and turbidity.



Site	Instrument and sensors	Frequency
Inner fjord 	RBR Concerto³, 9 m Temperature, salinity, pressure/depth, turbidity, PAR	5 min
Outer fjord 	RBR Maestro³, 18 m Temperature, salinity, pressure/depth, turbidity, PAR, fluorescence, dissolved oxygen.	30 min



Figure 2.2.1. Map of Young Sound with positions of the two INTAROS funded instruments

The two new instruments were placed on wired moorings on the sea floor. At the outer station, the instrument was placed on the existing wire thus complementing the ongoing time series of data from two instruments placed at 48 and 35 m depth.

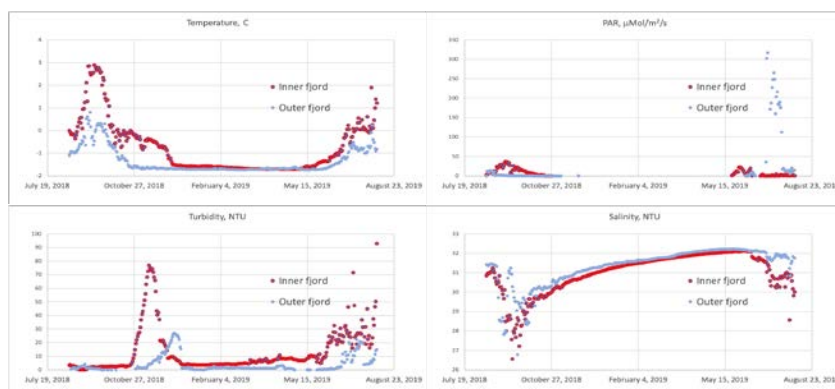


Figure 2.2.2. Daily average values of water temperature, underwater light (photosynthetic available radiation, PAR), turbidity and salinity at two sites in Young Sound.

To monitor sea ice conditions above the sensors, the monitoring program uses an autonomous camera system which provide a daily image of the outer. INTAROS funded another camera, to monitor conditions above the instrument in the inner fjord. Unfortunately, the new camera system, deployed in August 2018 was found broken in August 2019. It appears to have been damaged by musk oxen. The system was serviced and replaced and is hopefully taking daily images for the 2019-2020 season.

Spatial variation in coastal pCO₂. The partial pressure of CO₂ (pCO₂) of the surface water can be used to estimate air-sea exchange of CO₂. Coastal waters in general, and Arctic coastal waters specifically are responsible for a significant ocean uptake of atmospheric CO₂ (Laruelle et al. 2014). The capacity of Greenland fjords to take up CO₂, is influenced by the seasonal sea ice coverage and a combination of biological and physical processes (Meire et al. 2015, Sejr et al. 2011). The partial pressure of CO₂ is routinely measured in Young Sound, but to get a better estimate of variation among different fjord systems in Greenland, we wanted to look at spatial variation in summer surface pCO₂ values. Based on two coastal cruises to west Greenland fjords in 2016 and East Greenland fjords in 2018, we have made 746 observations of the pCO₂ in the upper 50 m distributed among 120 stations (Fig. 2.2.3). Measurements were done with a Contros HydroC pCO₂ instrument.

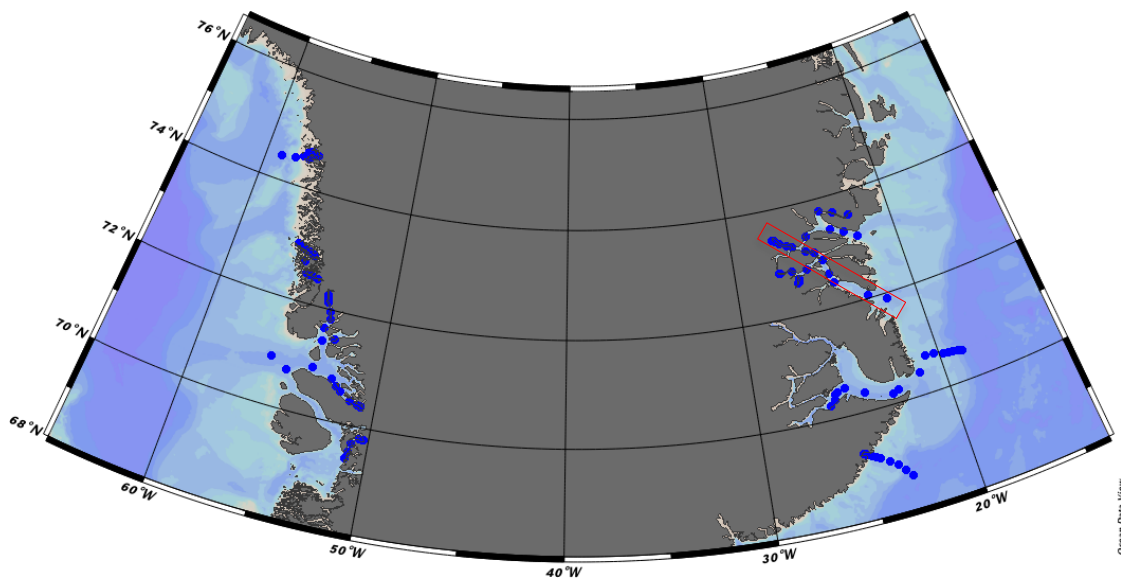


Figure 2.2.3. Sites where pCO₂ profiles have been measured in the upper 50 m. Red rectangle identifies the Kong Oscar Fjord transect.

2.2.2. Description of provided data

Seasonal data from Young Sound. The overview of specific sensors on each instrument and the factory provided initial accuracy estimate is provide in Table 2.2.1. Via the RBR provided software Ruskin (freely available at RBR homepage) used to communicate with the instrument and extract data a few additional parameters are calculated per default. Derived variables include salinity, speed of sound, depth and density for both instruments. Data for both instruments will be available at the open Greenland Ecosystem Monitoring Programme database (<https://data.g-e-m.dk>).

	Sensor	Accuracy
RBR Maestro³		
turbidity	Seapoint	±2%
PAR	Licor Spherical 193A	±2%
fluorescence	Turner Cyclops chl a	±2%
dissolved oxygen	RBRcoda ODO	Max of ±8 µM or ±5%
conductivity	Marine CT	±0.003mS/cm
pressure	RBR piezo guage	0.05% of full scale
temperature	Marine CT	±0.002 C
RBR Concerto³		
pressure	RBR piezo guage	0.05% of full scale
conductivity	Marine CT	±0.003mS/cm
temperature	Marine CT	±0.002 C
PAR	Licor Spherical 193A	±2%
turbidity	Seapoint	±2%

Table 2.2.1. List of sensors and factory estimated of initial accuracy.

Spatial variation in coastal pCO₂ The Contros instrument was deployed from the side of the ship with a online connection to a computer onboard. Usually the instrument takes 2-5 minutes to equilibrate to in situ conditions before a stable value can be read. Depth of each measurement was based on pre-set marks on the cable. The factory estimated accuracy is given to 0.5% of reading. Data will be presented in a scientific paper, where raw data will be made available and uploaded to the SOCAT data base. In Figure 2.2.4 is an example from a 260 km transect made along an East Greenland fjord showing that most of the surface water is undersaturated in pCO₂ and thus takes up CO₂ from the atmosphere.

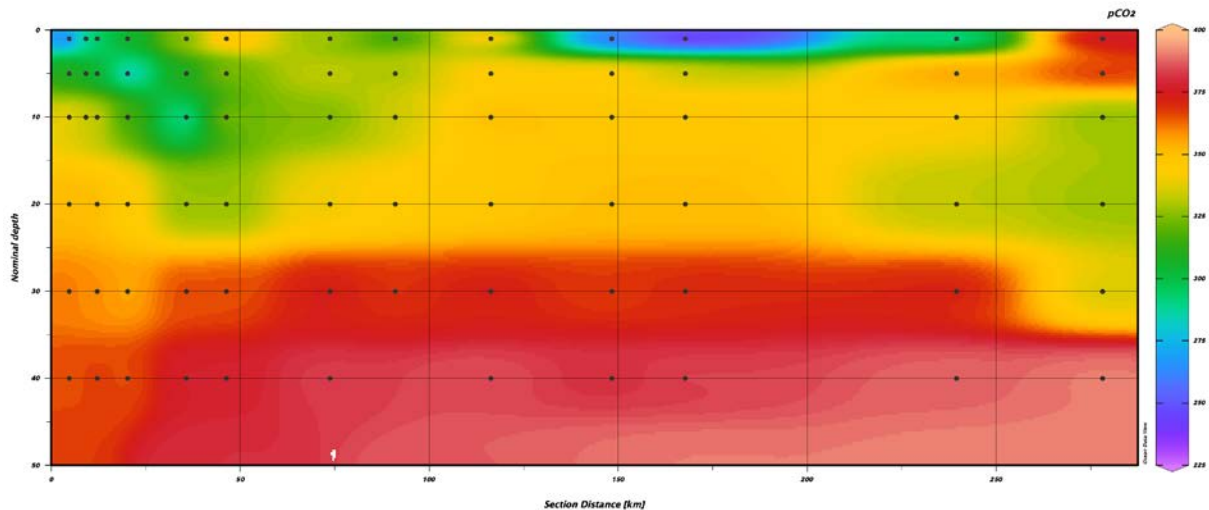


Figure 2.2.4. Partial pressure of CO₂ (pCO₂) from Kong Oskar fjord in East Greenland sampled in August 2018. see Fig. 2.2.3 for the location of the transect.

2.2.3. Plans for the final implementation

Seasonal data from Young Sound Two instruments of each version were purchased. Thus, when one instrument is retrieved after collecting for a full year it is replaced by a new, and can be brought home for service and re-calibration. When instruments were retrieved in August 2019, they were thus replaced by newly series and calibrated instruments. The added instrumentation is thus fully implemented in the monitoring program and is expected to provide data approximately 360 days a year. Data handling takes place with the existing monitoring data which after quality check is deposited on the open GEM data base.

Spatial variation in surface pCO₂ The obtained data will be presented in scientific papers, and include a comparison to observation in the GEM monitoring fjords, Young Sound and Godthaabsfjord where similar data are available. The obtained data will also be included in task 6.5.

2.3. FMI

Contributors: Roberta Pirazzini, Teijo Arponen

2.3.1. Results of the first operational implementation

The hardware and software components needed for the thermal and angular characterization of the PROMICE pyranometers included in the Kipp and Zonen CNR1/CNR4 net radiometers were completed. The schematic representation of the rotatory stage used for the angular characterization, including the mechanical jigs required to attached the instruments, is shown in Figure 2.3.1.

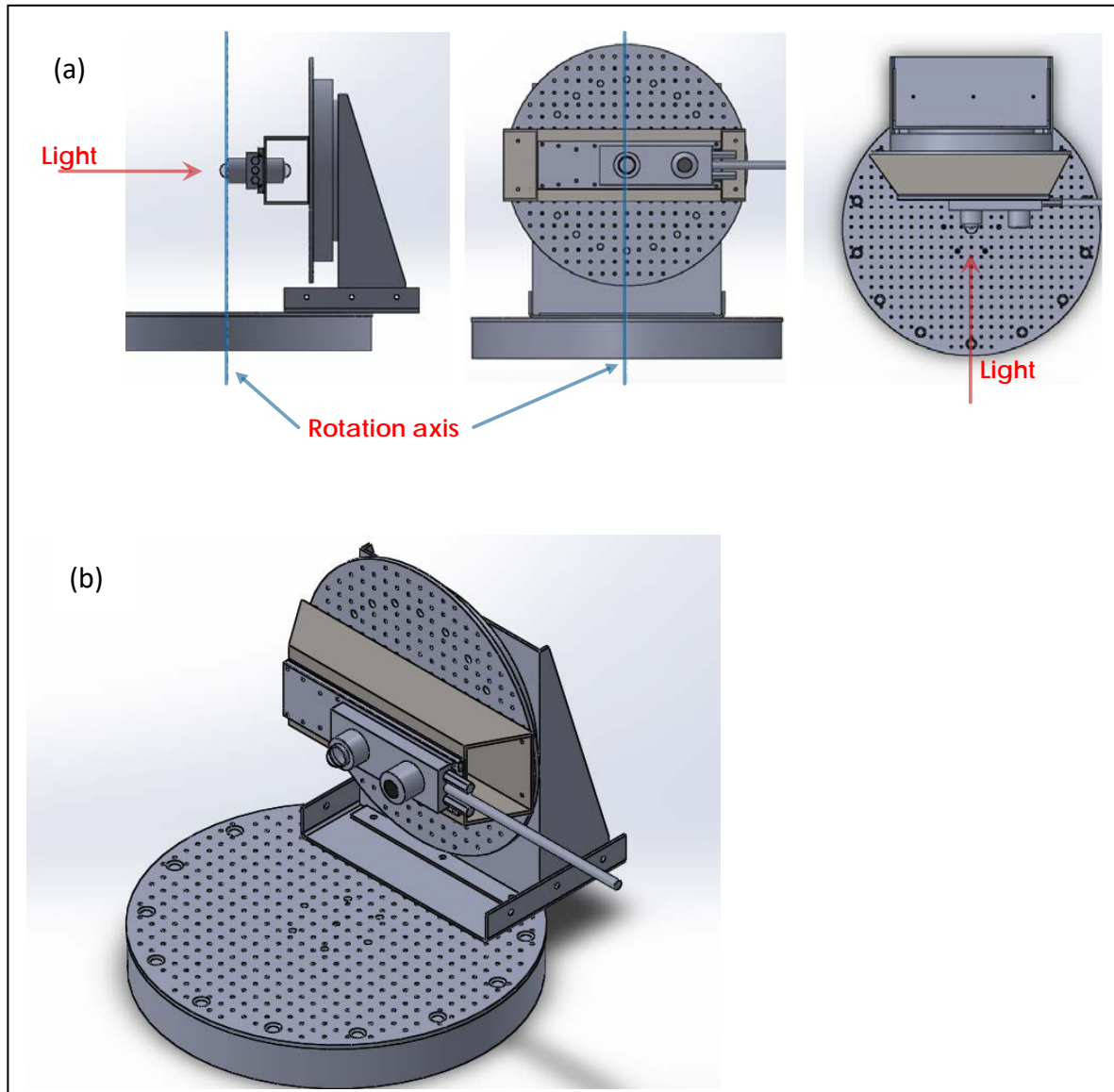


Figure 2.3.1. Schematic representation of the Kipp and Zonen SPN1 net radiometer attached to the two-axis rotatory stage: 2D views of the light path and of the rotation axes (a) and 3D view of the system.

A 250 W calibrated lamp is used to perform the angular and thermal characterization. In addition to the mechanical components, also the software that controls the characterization experiments in the temperature controlled chamber and on the two-axis rotatory stage was completed. Unfortunately, the unexpected breaking of the cooling system of the temperature

controlled chamber and the consequent need of total replacement of many components caused a one-year delay in the characterization work.

2.3.2. Description of provided data

The angular dependent correction that needs to be applied to reach the perfect cosine response of the pyranometers, as well as the temperature dependency of the pyranometers' sensitivity, will be provided in the format of ascii tables.

2.3.3. Plans for the final implementation

The net radiometers recovered from the PROMICE network during summer 2019 will be characterized in winter 2020-2021.

2.4. UPM

Contributors: Francisco Navarro, Javier Lapazaran

2.4.1. Results of the first operational implementation

The new ground-penetrating radar (GPR) system, VIRL8, is actually a combination of components from the former system, VIRL7 (Vasilenko et al., 2011, 2012), and new, improved components, all of which are fully interchangeable, though those of the newer version have improved capabilities. The radar system is described with detail in Section 3.4 of Deliverable 3.1. Basically, the radar system consists of two main parts: transmitter (TX) and receiver (RX), both connected by an optical synchronization link. The RX includes the control and recording unit (CRU) and a receiver amplifier (RA). Additionally, the system includes two antennas, external batteries, and optionally a GPS receiver and an odometer.

Some of the new components (in particular the CRU) are still in development phase, but those already developed (even if partially) have been lab-tested and field-tested successfully. We initially planned fieldwork in Greenland in spring 2019. However, due to logistic reasons, this campaign could not be accomplished, and we did instead field testing of the equipment taking advantage of an already-scheduled field campaign in Livingston Island, Antarctica, in December 2018-January 2019, with the logistic support of the Spanish Antarctic Station Juan Carlos I and a helicopter provided by the Colombian Navy.

In particular, the radar profiling was done on 14 January 2019, using a Bell 412 helicopter on board the "ARC 20 de Julio" ship of the Colombian Navy.



Figure 2.4.1. GPR system deployed in the Antarctic Campaign 2018-19 in Livingston Island, Antarctica: transmitter (upper, left panel), receiver (upper, right panel) and wooden frame (lower panel) for transportation of the radar system hanging under a helicopter. The wooden frame holds the transmitter and receiver subsystems in the green boxes and the transmitting and receiving antennas along the main arm of the frame.

2.4.2. Description of provided data

Glacier ice-thickness was measured, using the 20 MHz GPR system, along ca. 200 km of radar lines, shown in Fig. 2.4.2.a. An ice-thickness measurement was taken every 0.2-0.3 s, which, considering a helicopter velocity of ca. 75 km/h, means an ice thickness measurement every ca. 5 m. The error in ice thickness depends on an assumption of the error in radio-wave velocity in ice, and is point-dependent (proportional to the thickness), but its lower bound is the radar system resolution, dependent on radar frequency, which is ca. 4 m for a 20 MHz system. A sample of the raw data collected is displayed in Fig. 2.4.2.b. The main processing steps (implemented using ReflexW software, <https://www.sandmeier-geo.de/reflexw.html>) consisted of bandpass filtering, normal move-out correction, amplitude correction and migration (Navarro and Eisen, 2000). Deconvolution was not used because our pulse duration is small (~25 ns) and thus there is no need to shorten it. For preliminary time-to-thickness conversion, we used a constant radio-wave velocity of 0.168 m ns^{-1} , but this might be changed at a later stage, perhaps considering slightly different velocities for different zones.

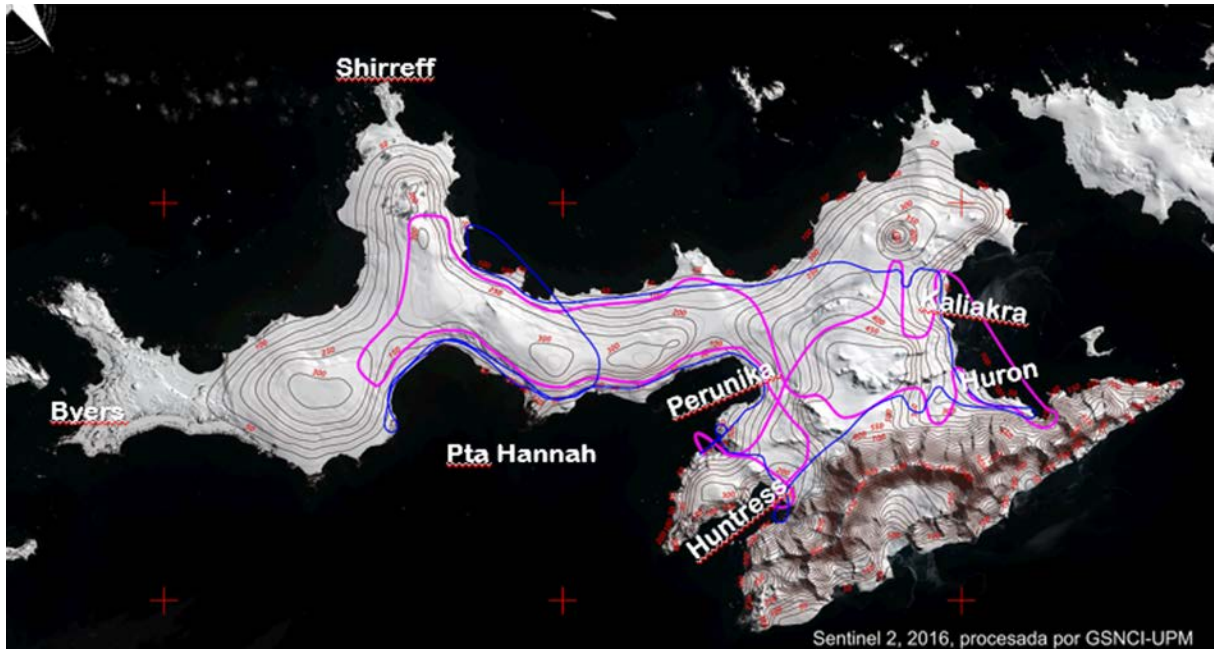


Figure 2.4.2.a. GPR lines performed on Livingston Island (blue lines), Antarctica, in January 2019, using VIRT 20 MHz radar system. The magenta lines represent the GPR lines originally planned.

The collected data, upon use in scientific publications, will be stored and made publicly available, together with the associated metadata, through the Glacier Thickness Database (GlaThiDa Consortium, 2019; https://www.gtn-g.ch/data_catalogue_glathida/), maintained by the World Glacier Monitoring Service (WGMS) for the Global Terrestrial Network for Glaciers (GTN-G).

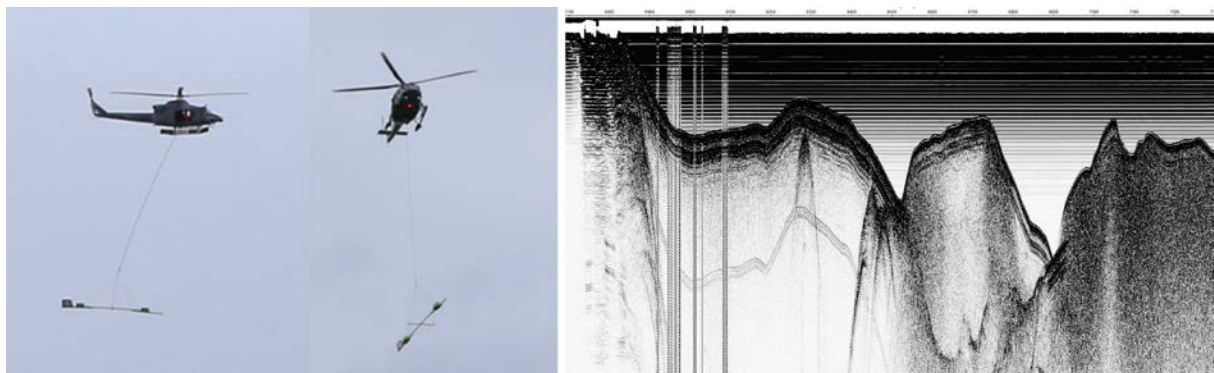


Figure 2.4.2.b. Left: two images of the GPR system on the frame hanging from the helicopter. Right: a sample of raw (unprocessed) data obtained during the GPR profiling on Livingston Island.

2.4.3. Plans for the final implementation

A fieldwork campaign is planned in the vicinity of Qaanaaq, north-western Greenland, in early spring 2020. The work will be aimed at collecting ice-thickness data near the calving front of Bowdoin Glacier and the highly-crevassed fronts of other neighbouring glaciers (e.g. Verhoeff, Hubbard, Tracy, Heilprin), where GPR operation from the glacier surface is not possible or, if possible, involves a high risk. The participants in the planned fieldwork will be Dr. Javier Lapazarán and Dr. Jaime Otero. For profiling, the 20 MHz radar system will be transported by a helicopter from the neighbouring Thule station. The fieldwork is planned for early spring (end of March or beginning of April 2020), well before the onset of melting, which would obscure the bed reflections due to backscattering from meltwater at the glacier surface or in the near-surface zone.

Bowdoin Glacier has been selected as target glacier because of the availability of both glaciological and oceanographic data (mostly collected by Japanese and Swiss colleagues) that will allow modelling the coupled glacier-fjord system, in order to determine the submarine melting at the glacier front and the calving rate. Ice-thickness at the front of neighbouring glaciers will be used, together with ice-surface velocities determined from satellite remotely-sensed synthetic aperture radar (SAR) data, to estimate the ice discharge from these glaciers to the ocean. These studies are fundamental to estimate the contribution from glaciers to sea-level rise. This work will be part of INTAROS Task 6.4 (Natural hazards in the Arctic), and the basis of one of its deliverables (D6.17-Ice discharge from glaciers to the ocean: Model-based demonstration of calculations of ice discharge from selected glaciers to the ocean, aimed to predict the contribution of glaciers to sea level rise). The ice-thickness data will also contribute to the development of the future product for the Greenland ice sheet mass loss delivered by GEUS in Task 6.4, where it will be key to pinpoint the spatial structure of the freshwater release from the ice sheet to the fjord/ocean system which in turn governs the impact of the changing freshwater flux on the marine ecosystem.

2.5. CNRS-IUEM

Contributors: Laurent Chauvaud

2.5.1. Results of the first operational implementation

In August 2015 and 2016, underwater acoustic recordings with RTSYS recorders equipped with up to 4 hydrophones at several locations in the Young Sound Fjord. Two types of recordings were made:

- 24 hours recording using a 4-channel RTsys recorder moored in various environments to record biological activity and ice sounds.

- short term recordings (10 minutes to 1 hour) using a 1 channel RTsys recorder deployed on a drifting buoy next to walruses (Sand Island, Basalt Island).

During the last cruise in May 2018, the acoustic dataset was completed with recordings of several days in different bottom types.

The Greenland experiment was a “test” phase. Since May 2018, equipments (described above) have been deployed at Kongsfjorden, Svalbard (see INTAROS report D3.8).

2.5.2. Description of provided data

The available acoustic dataset has a good spatial coverage. However the temporal coverage is very limited with data collected only during the summer months for small periods of time.

2.5.3. Plans for the final implementation

Acoustic efforts are now focused on experiments in Svalbard. There are no new missions planned in Greenland. The recorded data will be used as a point of comparison with the data acquired in Svalbard (postdoc position in 2020).

2.6. CNRS-Takuvik

Contributors: Marcel Babin, Claudie Marec

2.6.1. Results of the first operational implementation

The contribution of **CNRS-TAKUVIK** is made through the monitoring of the biogeochemical properties of the Baffin Bay with the deployment of a fleet of bio-Argo floats dedicated to navigate in ice-infested waters. The overarching goal is to understand the processes that control the Arctic PSB (Phytoplankton Spring Blooms) as it expands northward and to determine its fate in the ecosystem by investigating its related carbon fluxes. The long-term objective is to determine the fate of the PSB in a changing AO (Arctic Ocean).

Year-long high-frequency time series of phytoplankton phenology and its drivers are required and BGC Argo floats are the complementary tools to remote sensing and oceanographic cruises for these studies.

To study the onset of a PSB event under melting sea ice in May to its conclusion within the SIZ in July, Takuvik has deployed BGC Argo floats (called Proice, dedicated to polar environments) in Baffin Bay since the beginning of the program. The deployments are staggered in time (5 in Spring 2016 with 4 in Baffin Bay, 7 in Summer 2017, 2 in Summer 2018, 2 in Summer 2019). Five deployments are scheduled in Summer 2020 (in the meantime, some floats have been recovered and re-fitted to be deployed again).

The study focuses on Baffin Bay, which involves navigational challenges for floats in terms of bathymetry, ice coverage and circulation. Although the Proice floats are adapted to ice-infested waters, the experiment remains a real challenge. The real reason for the loss of some floats, at the beginning of the experiment remains unexplained, but we could diagnostic a mismanagement of the grounding in the firmware that lead to three losses at least (this problem has been fixed).

In spite of this, more than 1900 profiles have been acquired so far with unprecedented sets of data with series measured under ice during wintertime (two winters under ice for takapm016b, one winter under ice for takapm011b, takapm017b, takapm020b). Table 2.6.1 gives the amount of profiles acquired per float.

Additionally, in situ observations of the optical, physical and chemical properties of the sea-ice will be documented through new miniaturised sensors being developed at Takuvik. These instruments will be mounted on an ice endoscope in 2020.

2.6.2. Description of provided data

Pro-ice are BGC floats (biogeochemical) equipped with a CTD (conductivity-temperature-depth) Seabird41 unit, an Aanderaa 4330 oxygen optode mounted on a 30 cm stalk, a Wetlabs REM-A (combining OCR504 radiometer (380 nm, 412 nm, 490 nm and PAR) and ECOTriplet for the observation of chlorophyll-*a* fluorescence, colored dissolved organic matter, and particle backscattering at 700 nm (bbp), as well as a Satlantic SUNA V2 sensor. This payload gathers five of the six core Biogeochemical Argo variables.

The floats profile at various rates according to the season with a daily rate since mid-July until mid-November (or earlier depending on ice cover), then with a frequency of one to two weeks.

Data acquired of the various parameters (Pressure, Temperature, Salinity, Dissolved Oxygen, Radiometry, chl a Fluorescence, CDOM Fluorescence, particles abundance and nitrates are precious (up to 2 years) time-series. They are available in real time (RT) and free of access on the ARGO data center.

To upload RT data: <ftp://ftp.ifremer.fr/ifremer/argo/dac/coriolis/>

to visualize data: <http://www.argodatamgt.org/Access-to-data/Argo-floats-dashboard> or

<https://fleetmonitoring.euro-argo.eu/dashboard>

Data go then through the process of the quality control for each parameter. Data will later be available in the DM (delayed mode) in the ARGO data center.

Table 2.6.1 (profiles per PROICE float)

	WMO	1st profile	last profile	nbr profiles	Issue /comment
takapm014b	6902668	09/04/2016	31/10/2016	99	Disappeared during 1st winter
takapm005b	4901803	09/04/2016	31/10/2016	98	Disappeared during 1st winter
takapm009b	6902667	09/07/2016	31/10/2016	99	Disappeared during 1st winter
takapm013b	4901802	09/07/2016	31/10/2016	98	Disappeared during 1st winter
takapm019b	4901801	30/05/2016	25/05/2017	363	(no BGC- payload only O2)
takapm008b	6902669	20/07/2017	03/11/2017	102	Disappeared during 1st winter
takapm012b	4901805	20/07/2017	12/08/2018	124	Recovered – refit
takapm006c	4901804	20/07/2017	29/07/2017	12	Lost after grounding
takapm015b	6902670	20/07/2017	05/11/2017	113	Surface-blocked on Last descent
takapm017b	6902829	23/07/2017	9/04/2018	106	Destroyed upon recovery
takapm007b	6902666	23/07/2017	27/09/2017	70	Lost after grounding
takapm016b	6902671 6902953	23/07/2017	29/7/2019	185	Remote firmware upgrade (change of WMO)
takapm020b	6902897	17/7/2018	12/10/2019	186	Recovered for refit
takapm011b	6902896	17/07/2018	31/05/2019	133	Flooded
takapm018b	6902967	14/07/2019	-	115 to date	
takapm004b	4901806	17/07/2019	02/09/19	8	Recovered for maintenance and refit

2.6.3. Plans for the final implementation

Five more deployments are planned for 2020. One of these floats will be equipped with a new sensor dedicated to measure particle size abundance (UVP6 by Hydroptics). This will give a complementary information to characterize the ecosystem. The implementation of this sensor will be a “premiere” on an ARGO float in Arctic.



Figure 2.6.1. Proice float equipped with an UVP6- picture courtesy LOV.

Depending on the recoveries of floats, additional deployments are envisaged in 2021.

The automatizing of the in situ observations in the location near the village of Qikiqtarjuaq would be made possible through the deployment of a mooring with a bio-optical payload similar to the sensors aboard the BGC-Argo floats. These automated measurements would be complemented by regular in situ observations of the physical, chemical and biological properties measured through an independent set of bio-optical sensors and on discrete water samples.

3. Future plans for the final implementation of the observing system

The future deployment plans for each of the observing systems are described in detail in the subsections of Section 2 above by each partner. Below is a summary in Table 3.1 to provide a fast overview of these plans.

Table 3.1. Summary of future plans.

Partner		Activity	Deployment plans & recommendations
GEUS		SWE on ice sheet	Based on the results of the first deployment, we plan to fine-tune the instrument parameters and develop a solution to the power consumption/supply which is currently inadequate for wintertime operation
		Precise positioning on ice sheet	Remaining GNSS units will be produced and the communication issues with the Campbell logger addressed. Subsequently, the new GNSS units will be implemented at the selected PROMICE and GEM sites visited in 2020 as part of routine maintenance
		Tilt & azimuth of radiometers	Remaining tilt/azimuth units will be produced and the communication issues with the Campbell logger addressed. Subsequently, the new tilt/azimuth units will be implemented at the PROMICE and GEM sites visited in 2020 as part of routine maintenance
		Rain gauges on ice sheet	Experimental deployment of rain gauges is continued through 2020, with implementation of a new AWS system including a rain gauge at all >20 PROMICE locations starting in 2021. The implementation phase of this new AWS system is expected to be on the order of 4 years
AU		Snow on sea ice	When instruments are retrieved, they are replaced by new and calibrated instruments. The added instrumentation is thus fully implemented in the monitoring program and is expected to provide data approximately 360 days a year
		pCO ₂ & acidification	The retrieved data will form the basis of scientific publications and be made available on the open GEM database
FMI		Radiometer characterization	The net radiometers recovered from the PROMICE network during summer 2019 will be characterized in winter 2020-2021
UPM		GPR development	A fieldwork campaign is planned at Bowdoin Glacier in the vicinity of Qaanaaq, north-western Greenland, in early spring 2020

CNRS-IUEM		Passive acoustics	Acoustic efforts are now focused on experiments in Svalbard. There are no new missions planned in Greenland. The recorded data will be used as a point of comparison with the data acquired in Svalbard (postdoc position in 2020)
CNRS-Takuvik		Under-ice monitoring	Five more deployments are planned for 2020. One of these floats will be equipped with a new sensor dedicated to measure particle size abundance. Depending on the recoveries of floats, additional deployments is envisioned in 2021.

4. Summary

The work done in WP2 to obtain an overview of Arctic observation systems and the parameters, includes reports on present capabilities, gaps and exploitation which points to a significant potential for increased synergy within and between different spheres. This report only details work done within INTAROS in one of the reference sites, Coastal Greenland, but serves as a useful example of what may be accomplished over time on a larger scale. Cutting across established fields of research, bridging widely different applications, acknowledging the transnational character of the Arctic climate change challenge, INTAROS proves how we can make better use of our monitoring resources and make a focused effort to address the most critical observational gaps.

The majority of the actions reported here consist of improvement of monitoring system parameter coverage by adding existing sensors already available. A few actions report on actual technical improvement of sensors, like the VIRL ice-penetrating radar system of UPM, the assembly of a GNSS precise-positioning device suitable for automated measurements in extreme conditions and the collaboration between FMI and GEUS on improving the precision of shortwave radiation measurements on the Greenland ice sheet.

Overall, the Task 3.1 actions at the Coastal Greenland reference site deals with the impact of changes in the Arctic water and ice cycle on the physical and biological environment. Starting on the ice sheet by monitoring the amount of snow and rain precipitation, improving albedo measurements to qualify meltwater formation modelling and conducting precise ice-velocity measurements. All these parameters increase confidence in the solid and liquid freshwater transport to the ice margin, where improved ice thickness measurements help characterize the transition of the ice and meltwater to the fjord systems and surrounding ocean. In this domain, the monitoring of the impact of the freshening on the marine ecosystem, the physical characteristics and the ocean CO₂-uptake is improved.

Below, in Table 4.1, an overview of the progress in Task 3.1 is provided.

Table 4.1. Progress in Task 3.1.

Partner	GEUS
Action	Snow-water equivalent on the ice sheet
Objective	To reduce uncertainty in meltwater output to the ocean
Instrument development	None, except power supply
Field deployment	Summer 2018 - 5 instruments at four locations on the Greenland ice sheet
Challenges	Insufficient power supply during winter/snow burial
First results	Raw data converted successfully to snow-water equivalent

Partner	GEUS
Action	Precise positioning of ice sheet stations
Objective	To calibrate satellite-derived ice velocity maps and numerical weather prediction
Instrument development	Yes, assembling new type of GNSS unit with antenna and communication/control
Field deployment	Summer 2019 (test unit)
Challenges	Complications in the communication between parts of the assembly caused delays in field deployment, limiting test deployment to one site in 2019
First results	Available by spring or summer 2020 (first visit to test site in Kobbefjord, Nuuk, Greenland)

Partner	GEUS
Action	New radiometer tilt and azimuth instrument for improved radiation correction
Objective	To correct the radiation measurements with improved tilt and new azimuth data, because automatic weather stations operating on ice cannot provide a stable level orientation of the radiometers
Instrument development	Yes, assembling new type of tilt/azimuth unit with communication and control
Field deployment	Summer 2019 (test unit)
Challenges	Problems with powering and interfacing to the ADIS16209 resulting in occasional lock-ups during testing, as well as difficulties implementing the planned serial communication using the SDI-12 protocol
First results	Available by spring or summer 2020 (first visit to test site in Kobbefjord, Nuuk, Greenland)

Partner	GEUS
Action	Rain gauges on ice sheet stations
Objective	To observe rain events and their magnitude on the ice sheet
Instrument development	None
Field deployment	Rain gauges deployed during and prior to the INTAROS effort from 2016 to Fall 2019, with four sites currently in field operation
Challenges	The undercatch correction is substantial and needs field validation
First results	First corrected datasets for rain on the ice sheet is currently compared to results from a Japanese regional climate model

Partner	AU
----------------	----

Action	Snow cover on sea ice
Objective	To study the impact of freshening on the marine ecosystem
Instrument development	None
Field deployment	Aug 2018 – Aug 2019
Challenges	A new camera system to monitor conditions above the instrument in the inner fjord, deployed in August 2018 was found broken in August 2019. It appears to have been damaged by musk oxen. The system was serviced and replaced and is hopefully taking daily images for the 2019-2020 season
First results	CTD data successfully retrieved from the instruments deployed in Aug 2018

Partner	AU
Action	Surface pCO ₂ and ocean acidification
Objective	To study the impact of freshening on CO ₂ -uptake of the ocean
Instrument development	None
Field deployment	Two coastal cruises in West Greenland 2016 and East Greenland 2018
Challenges	None
First results	So far 746 observations of the pCO ₂ in the upper 50 m distributed among 120 stations

Partner	FMI
Action	Instrument characterization of in-situ ice sheet albedo measurements
Objective	To obtain improved validation of satellite albedo products
Instrument development	Yes, entirely new laboratory facility constructed
Field deployment	N/A
Challenges	The cooling system of the temperature controlled chamber broke and the consequent need of total replacement of many components caused a one-year delay in the characterization work
First results	None yet

Partner	UPM
Action	Improvement of ice-penetrating radar system
Objective	To generate ice thickness data over ice-sheet outlet glaciers
Instrument development	Yes
Field deployment	January 2019, testing the system (Livingston Island, Antarctica)
Challenges	Initially planned fieldwork in Greenland in spring 2019. However, due to logistic reasons, this campaign could not be accomplished. It has been necessary to re-use some modules from the existing radar in the development of the new system VIRL8
First results	Test flights delivered 200 km of good radar profiles over ice, proving the concept of the new helicopter-borne radar system in the field

Partner	CNRS-IUEM
Action	Passive acoustics for characterization of both physical and biological parts of the marine ecosystem
Objective	To study the ice-driven dynamics of Arctic coastal ecosystems

Instrument development	None
Field deployment	Aug 2015, Aug 2016, May 2018
Challenges	None
First results	Acoustic datasets retrieved

Partner	CNRS-Takuvik
Action	Improvement of under-ice monitoring
Objective	To observe spring bloom and bio-optical/-geochemical properties
Instrument development	None
Field deployment	Pro-ice BGC Argo floats deployed: five in Spring 2016 (with four in Baffin Bay), seven in Summer 2017, two in Summer 2018, two in Summer 2019.
Challenges	Although the Pro-ice floats are adapted to ice-infested waters, the experiment remains a real challenge. The real reason for the loss of some floats, at the beginning of the experiment remains unexplained, but we could diagnostic a mismanagement of the grounding in the firmware that lead to three losses at least (this problem has been fixed).
First results	More than 1900 profiles have been acquired so far with unprecedented sets of data with series measured under ice during wintertime

The majority of the technical and system design developments have been implemented and instruments deployed over the 2018 and 2019 field seasons. Results so far underline the challenges of operating in a severe and remote environment, with some instruments lost or damaged during field deployment, but also hard-earned success in retrieving unprecedented datasets of key physical, biological and biochemical parameters with innovative instrumentation.

Several of the system improvements and datasets reported here provide the basis for activities in WP6: *Applications of IAOS towards stakeholders*, which is focused on delivering demonstration products from the iAOS, more specifically Task 6.4 *Natural hazards in the Arctic* and Task 6.5 *Arctic greenhouse gases*.

5. Literature

Box, J.E., M. Niwano, R.S. Fausto, D. Van As, A.P. Ahlstrøm, Greenland precipitation measurements in support of glaciological applications, Geological Survey of Denmark and Greenland Bulletin, (in preparation)

Box, J. E., Fettweis, X., Stroeve, J. C., Tedesco, M., Hall, D. K., and Steffen, K.: Greenland ice sheet albedo feedback: thermodynamics and atmospheric drivers, *The Cryosphere*, 6, 821–839, <https://doi.org/10.5194/tc-6-821-2012>, 2012.

- Goodison, B.E., Louie, P.Y.T., and Yang, D. (1998): Solid Precipitation Measurement Intercomparison, WMO, 872.
- Holding, J. M., Markager, S., Juul-Pedersen, T., Paulsen, M. L., Møller, E. F., Meire, L., & Sejr, M. K. (2019). Seasonal and spatial patterns of primary production in a high-latitude fjord affected by Greenland Ice Sheet run-off. *Biogeosciences*, 16(19), 3777-3792.
- Krause-Jensen, D., Marbà, N., Olesen, B., Sejr, M. K., Christensen, P. B., Rodrigues, J., Renaud, P.E., Balsby, T.J.S. & Rysgaard, S. (2012). Seasonal sea ice cover as principal driver of spatial and temporal variation in depth extension and annual production of kelp in Greenland. *Global Change Biology*, 18(10), 2981-2994.
- Laruelle, G. G., Lauerwald, R., Pfeil, B., & Regnier, P. (2014). Regionalized global budget of the CO₂ exchange at the air-water interface in continental shelf seas. *Global biogeochemical cycles*, 28(11), 1199-1214.
- Meire, L., Sjøgaard, D. H., Mortensen, J., Meysman, F. J. R., Soetaert, K., Arendt, K. E., Juul-Pedersen, T., Blicher, M.E. & Rysgaard, S. (2015). Glacial meltwater and primary production are drivers of strong CO₂ uptake in fjord and coastal waters adjacent to the Greenland Ice Sheet. *Biogeosciences*, 12(8), 2347-2363.
- Navarro, F. J. and Eisen, O. (2010). Ground Penetrating Radar. In P.Pellikka and W.G. Rees (eds.): Remote sensing of glaciers – techniques for topographic, spatial and thematic mapping, pp. 195-229. CRC Press, Leiden.
- Niwano, M., Aoki, T., Matoba, S., Yamaguchi, S., Tanikawa, T., Kuchiki, K., and Motoyama, H.: Numerical simulation of extreme snowmelt observed at the SIGMA-A site, northwest Greenland, during summer 2012, *The Cryosphere*, 9, 971–988, <https://doi.org/10.5194/tc-9-971-2015>, 2015. GlacThiDa Consortium (2019). Glacier Thickness Database 3.0.1. World Glacier Monitoring Service, Zurich, Switzerland, doi: 10.5904/wgms-glathida-2019-03.
- Sejr, M. K., Krause-Jensen, D., Rysgaard, S., Sørensen, L. L., Christensen, P. B., & Glud, R. N. (2011). Air—sea flux of CO₂ in arctic coastal waters influenced by glacial melt water and sea ice. *Tellus B: Chemical and Physical Meteorology*, 63(5), 815-822.
- Vasilenko E. V., Machío F., Lapazaran J. J., Navarro F. J. and Frolovskiy K. (2011). A compact lightweight multipurpose ground-penetrating radar for glaciological applications. *Journal of Glaciology*, 57(206), 1113-1118, doi: 10.3189/002214311798843430.
- Vasilenko, E. V., Machío, F., Frolovskiy, K., Navarro, F. J. and Lapazaran, J. J. (2012). Patent ES 2 356 547 B2: Unidad de control y registro digital para un georradar de aplicación específica en glaciología. (Digital recording and control unit for a georadar of specific use in glaciology). *Oficina Española de Patentes y Marcas*.

----- END of DOCUMENT-----



INTAROS

This report is made under the project
Integrated Arctic Observation System (INTAROS)
 funded by the European Commission Horizon 2020 program
 Grant Agreement no. 727890.



Project partners:

